m^6A demethylase ALKBH5 promotes tumor cell proliferation by destabilizing IGF2BPs target genes and worsens the prognosis of patients with non-small-cell lung cancer

Kazuo Tsuchiya[1,2], Katsuhiro Yoshimura[1,2], Yuji Iwashita[1], Yusuke Inoue[1,2], Tsutomu Ohta[1,3], Hirofumi Watanabe[1,2], Hidetaka Yamada[1], Akikazu Kawase[4], Masayuki Tanahashi[5], Hiroshi Ogawa[6], Kazuhito Funai[4], Kazuya Shinmura[1], Takafumi Suda[2], Haruhiko Sugimura[1*].

1. Department of Tumor Pathology, Hamamatsu University School of Medicine, Hamamatsu, Japan

2. Second Division, Department of Internal Medicine, Hamamatsu University School of Medicine, Hamamatsu, Japan

3. Department of Physical Therapy, Faculty of Health and Medical Sciences, Tokoha University, Hamamatsu, Japan

4. First Department of Surgery, Hamamatsu University School of Medicine, Hamamatsu, Japan

5. Division of Thoracic Surgery, Respiratory Disease Center, Seirei Mikatahara General Hospital, Hamamatsu, Japan

6. Department of Pathology, Seirei Mikatahara General Hospital, Hamamatsu, Japan

Corresponding author:

Haruhiko Sugimura, MD, Ph.D., Department of Tumor Pathology, Hamamatsu University School of Medicine, 1-20-1 Handayama Higashi-ku, Hamamatsu, Shizuoka 431-3192 Japan. Tel: +81-53-435-2220; Fax: +81-53-435-2225; Email: hsugimur@hama-med.ac.jp

Abstract

The modification of N^6-methyladenosine (m^6A) in RNA and its eraser ALKBH5, an m^6A demethylase, play an important role across various steps of human carcinogenesis. However, the involvement of ALKBH5 in non-small-cell lung cancer (NSCLC) development remains to be completely elucidated. The current study revealed that the expression of ALKBH5 was increased in NSCLC and increased expression of ALKBH5

worsened the prognosis of patients with NSCLC. *In vitro* study revealed that ALKBH5 knockdown suppressed cell proliferation ability of PC9 and A549 cells and promoted G1 arrest and increased the number of apoptotic cells. Furthermore, ALKBH5 overexpression increased the cell proliferation ability of the immortalized cell lines. Microarray analysis and western blotting revealed that the expression of CDKN1A (p21) or TIMP3 was increased by ALKBH5 knockdown. These alterations were offset by a double knockdown of both ALKBH5 and one of the IGF2BPs. The decline of mRNAs was, at least partly, owing to the destabilization of these mRNAs by one of the IGF2BPs. In conclusions, the ALKBH5–IGF2BPs axis promotes cell proliferation and tumorigenicity, which in turn causes the unfavorable prognosis of NSCLC.

Keywords: Non-small-cell lung cancer (NSCLC), m^6A, ALKBH5, IGF2BPs, CDKN1A (p21), TIMP3

Background

Lung cancer, the incidence of which has continued to increase annually, remains the most frequently diagnosed cancer and leading cause of cancer-related death worldwide (1). Considering the rapid improvement in the treatment of lung cancer,

particularly non-small-cell lung cancer (NSCLC), physicians now have several options of personalized treatments targeting driver genes, such as EGFR mutations, ALK rearrangements, ROS1 rearrangements, and BRAF mutations or combination therapies comprising immunotherapy and anticancer drugs (2-6). However, despite the current advancements in precision medicine, NSCLC still exhibits poor long-term prognosis and high mortality rates owing to the rapid growth, metastasis, and infiltration of cancer. Therefore, identifying effective therapeutic targets that inhibit such malignant behaviors of NSCLC is urgently needed.

N^6-methyladenosine (m^6A), the most prevalent internal messenger RNA (mRNA) modification, controls various mRNA functions. The m^6A sites, which are widely distributed around the stop codons and 3′ untranslated regions (UTRs) of mRNAs, presumably exist in precursor mRNAs (7). Recent m^6A transcriptome analysis revealed that m^6A is predominantly present in the RRACU (R = A/G) consensus motif of mammals (8). m^6A is reversibly catalyzed by a methyltransferase complex (writer) and demethylase (eraser). Accordingly, the methyltransferase complex comprises methyltransferase-like 3 and 14 (METTL3 and METTL14) with their cofactors Wilms tumor 1-associated protein (WTAP), VIRMA (KIAA1429), and RNA-binding motif protein 15 (RBM15) (9-12). Further, fat mass and obesity-related protein (FTO) and

AlkB homolog 5 (ALKBH5) have been identified as two eukaryotic demethylases that oxidatively demethylate m^6A with α-ketoglutarate as a substrate and Fe (II) as a coenzyme (13, 14). FTO is also involved in the demethylation of N^6,2′-*O*-dimethyladenosine (m^6A_m) whereas there is no other RNA than m^6A that is demethylated by ALKBH5 (15, 16). Moreover, m^6A-binding protein (reader protein), which recognizes m^6A, is involved in numerous biological processes in an m^6A-dependent manner. For instance, YT521-B homology (YTH) domain containing 1 (YTHDC1) and YTHDC2 promote alternative splicing and mRNA export from the nucleus to the cytoplasm (17, 18); heterogeneous nuclear ribonucleoprotein G (HNRNPG) alters RNA structures via RNA–protein interaction (19, 20); YTH domain family1 (YTHDF1), YTHDF3, METTL3, and eukaryotic initiation factor3 (eIF3) regulate translation efficiency (21-24); and insulin-like growth factor 2 mRNA-binding proteins (IGF2BPs), YTHDF2, YTHDF3, and YTHDC2 alter mRNA stability (24-27).

Over the past few years, several researchers investigating the role of m^6A erasers in malignant tumors have revealed that m^6A eraser proteins play a critical role in oncogenesis. A number of previous studies have demonstrated that ALKBH5 exerts a cancer-promoting effect in glioblastoma, osteosarcoma, colon cancer, ovarian cancer, esophageal squamous cell carcinoma, endometrial cancer, and renal cell carcinoma

(28-34). In contrast, ALKBH5 has been reported to play a tumor-suppressing effect in hepatocellular carcinoma and pancreatic cancer (35, 36). Several studies on lung cancer have shown that FTO plays a cancer-promoting role through m^6A modification in lung squamous cell carcinoma and adenocarcinoma (37-39), whereas ALKBH5 inhibits NSCLC tumorigenesis by reducing YTHDFs-mediated YAP expression (40). Conversely, ALKBH5 had also been found to promote NSCLC progression by reducing TIMP3 stability (41) or stabilizing oncogenic drivers such as SOX2, SMAD7, and MYC (42). Thus, the precise role of ALKBH5 in NSCLC tumorigenesis across various conditions deserves further investigation.

Cell type and cell environment (e.g., during hypoxic conditions), as well as the m^6A target gene and its recognition protein (reader), have been found to affect RNA metabolism caused by ALKBH5 perturbation (43, 44). Therefore, m^6A-mediated gene expression regulated by ALKBH5 could result in various consequences in cancer cells, depending on the surrounding environment and other factors. Several studies regarding m^6A have focused on specific genes in the specific contexts, with their results showing that m^6A is involved in the mechanisms through which these specific genes are regulated. However, in actual human cancers, ALKBH5 catalyzes specific m^6A of numerous genes, which simultaneously alters several RNA and protein expressions

through RNA recognition by reader proteins, consequently causing numerous interactions between them *in vivo*. As such, systematically clarifying the association between m^6A modification and cancer development across each clinical and pathological setting is important. Furthermore, elucidating the significance of m^6A modification by ALKBH5 may facilitate the clinical usage of such molecules as therapeutic targets. Therefore, the current study aimed to examine the role of m^6A demethylase in NSCLC focusing on ALKBH5 and determine its association with downstream targets, including “readers” and “target genes.”

Methods

Immunohistochemistry

Resected NSCLC samples from Hamamatsu University School of Medicine and Seirei Mikatahara General Hospital were collected and named as the HUSM cohort. Tissue microarray (TMA) sections were analyzed using immunohistochemistry (IHC) as previously described (45). Cores of insufficient quality or quantity were excluded from the analysis. Antibodies for ALKBH5 (HPA007196, Atlas Antibodies, Stockholm, Sweden) and FTO (Ab124892, Abcam, Cambridge, UK) were diluted at 1:400, whereas those specific for EGFR E746-A750 deletion (#2085, D6B6, Cell Signaling Technology

126 [CST], Danvers, MA, USA) and EGFR L858R mutant (#3197, 43B2, CST) were
127 diluted at 1:100, followed by incubation at room temperature for 0.5 h. Protein
128 expression levels were then assessed using the H-score, which was calculated by
129 multiplying the percentage of stained tumor area (0%–100%) by the staining intensity
130 (scored on a scale of 0–3) to yield a value ranging from 0 to 300.
131
132 **Analysis of publicly available datasets**
133 We used the lung cancer database in the Kaplan–Meier plotter
134 (http://kmplot.com/analysis/index.php? p=service&cancer=lung) to analyze the
135 association between prognosis and ALKBH5 and FTO mRNA expression in NSCLC
136 cohorts. Data were downloaded on December 10, 2020. Kaplan–Meier curves for
137 overall survival (OS) were generated and stratified according to the median expression
138 of each mRNA. To assess the mRNA expression of ALKBH5 and FTO, data from the
139 Cancer Genome Atlas (TCGA) (NSCLC, Provisional) were downloaded from
140 cBioPortal (http://www.cbioportal.org/) on November 11, 2019. Expression data were
141 obtained in the form of RNA-seq by Expectation Maximization (RSEM).
142
143 **Immunofluorescence analysis**

144 Cells grown on coverslips were fixed with 4% paraformaldehyde and permeabilized
145 with 0.1% Triton X-100. After blocking with 5% bovine serum albumin in PBS (−) at
146 room temperature for 1 h, the cells were probed with primary antibodies against
147 ALKBH5 (HPA007196, Atlas Antibodies) and then incubated with a Goat anti-Rabbit
148 IgG (H + L) Cross-Adsorbed Secondary Antibody, Alexa Fluor 546 (#A-11010, Thermo
149 Fisher Scientific, Waltham, MA, USA). Nuclei were stained with ProLong® Gold
150 Antifade Reagent with DAPI (#8961, CST), after which the cells were imaged via
151 fluorescence microscopy using z-stack image reconstructions (BZ-9000; Keyence,
152 Osaka, Japan).

153

154 **Cell lines and transient knockdown with siRNA**

155 The human lung cancer cell lines H1299, H460, H2087, A549, ABC1, and H358 and
156 the human immortalized cell lines BEAS2B and HEK293 were obtained from Health
157 Science Research Resources Bank (Osaka, Japan) or the American Type Culture
158 Collection (Manassas, VA, USA). PC3 and PC9 lung cancer cells were purchased from
159 the Japanese Collection of Research Bioresources Cell Bank (Osaka, Japan) and
160 RIKEN BioResource Center (Tsukuba, Japan), respectively, whereas ACC-LC176 cells
161 were a kind gift from Dr. Takashi Takahashi (Nagoya University). RERF-LC-MS,

HLC-1, and LC-2/ad were kind gifts from Dr. Toshiro Niki (Tokyo University). Lung cancer cell lines were cultured in RPMI1640 medium (R8758, Thermo Fisher Scientific), whereas HEK293 cells were cultured in DMEM (D5796 MERCK, Darmstadt, Germany) containing 10% (vol./vol.) fetal bovine serum (FBS), 100 IU/mL penicillin G, and 100 μg/mL streptomycin. LHC9 (12680013, Thermo Fisher Scientific) was also used as a medium for BEAS2B cells. Cells were maintained in a 5% CO_2 and 95% air incubator at 37□. Silencer Select Pre-designed siRNA for ALKBH5 (siALKBH5: s29743, s29744, s29745, Thermo Fisher Scientific), FTO (siFTO: s28147, s28148, s28149, Thermo Fisher Scientific), IGF2BP1 (siIGF2BP1: s20916, s20917, Thermo Fisher Scientific), IGF2BP2 (siIGF2BP2: s20922, s20923, Thermo Fisher Scientific), IGF2BP3 (siIGF2BP3: s20919, s20920, Thermo Fisher Scientific), YTHDF2 (siYTHDF2: s28147, s28148, Thermo Fisher Scientific), CDKN1A (siCDKN1A: s145, s147, Thermo Fisher Scientific), TIMP3 (siTIMP3: s14147, s14148, Thermo Fisher Scientific), and Silencer Select Negative control (siNC: 4390843, Thermo Fisher Scientific) were purchased for transient knockdown. More than two different sequences were used for one target gene to minimize off-target effects. Cells were cultured for 24 h before transfection, after which they were transfected with 15 nM of final siRNA concentrations using Opti-MEM (31985070,

Gibco, Dublin, Ireland) and Lipofectamine® 2000 (11668019, ThermoFisher). The cells were then used for further assays at 48–96 h after transfection. When no siRNA sample number was available, siRNA no. 1 (#1) and siRNA no. 3 (#3) were pooled for ALKBH5 unless otherwise specified. siIGF2BP1, siIGF2BP2, siIGF2BP3, siYTHDF2, siCDKN1A, and siTIMP3 were pooled for all transfections.

Generation of Retro-X Tet-On inducible cell lines overexpressing ALKBH5

The retroviral plasmid pRetroX-TetOne puro (634307, Clontech, Mountain View, CA, USA) was amplified using NEB Stable competent *Escherichia coli* (high efficiency) (C3040H, NEW ENGLAND BioLabs, Ipswich, MA, USA). The full-length ALKBH5 sequence (NM_017758), which was confirmed using Sanger sequencing, was subcloned into pRetroX-TetOne puro vector using EcoRI and BglII restriction sites (pRetroX-TetOne puro-ALKBH5). Retroviral supernatants were produced using the GP2-293 packaging cell line (Clontech), in which pRetroX-TetOne puro empty vector or pRetroX-TetOne puro-ALKBH5 were each cotransfected with the envelope vector VSV-G using Xfect transfection reagent (Clontech). BEAS2B, HEK293, PC9, and A549 cells were transfected for 24 h using 4 μg/mL polybrene (H9268, Sigma-Aldrich, St. Louis, MO, USA). Puromycin selection (0.5–1.5 μg/mL) began 48 h after transfection

and lasted for 3 days until all nontransfected cells had died. In subsequent experiments, Retro-X cells were induced with 0.1–100 ng/mL of doxycycline (DOX) diluted in culture media upon cell seeding for 24–96 h. Cells transfected with pRetroX-TetOne puro-ALKBH5 with 100 ng/mL DOX were designated as ALKBH5-overexpressed (OE) cells, whereas those infected without DOX were designated as negative control (NC) unless otherwise noted.

RNA isolation and quantitative-polymerase chain reaction (qPCR)

Total RNA was extracted using the RNeasy Plus Mini Kit (#74136, QIAGEN, Hilden, Germany) according to the manufacturer's instructions, with the total RNA concentration calculated using Nanodrop (NanoDrop1000, Thermo Fisher Scientific). cDNA was synthesized from 1 μg of total RNA using the ReverTra Ace qPCR RT Master Mix (FSQ-201, TOYOBO) or SuperScript III Reverse Transcriptase (1080044, Thermo Fisher Scientific) according to the manufacturer's instructions. qPCR reactions were performed on a Step One Plus Real-Time PCR System (Applied Biosystems, Thermo Fisher Scientific) using the THUNDERBIRD qPCR Mix (QPS-201, TOYOBO, Osaka, Japan). The relative RNA expression levels were calculated using the ΔΔCt method, with the levels normalized to glyceraldehyde 3-phosphate dehydrogenase

(GAPDH) mRNA. All amplicons were confirmed as a single product using agarose gel visualization and/or melting curve analysis. The applied primer sequences are listed in Table S1.

Protein isolation and western blotting

Total protein lysates were extracted from whole cells using 1× sodium dodecyl sulfate (SDS) sample buffer. The Pierce BCA Protein Assay Kit (Cat#23225, Thermo Fisher Scientific) was used to determine the protein concentration. All proteins were separated using SDS-polyacrylamide gel electrophoresis and transferred to PVDF Blotting Membrane (P 0.45, A29532146, GE healthcare Life science, Chicago, IL, USA) using the Trans-Blot Turbo Cassette (Bio-Rad, Hercules, CA, USA). Blocking One (03953, Nacalai, Kyoto, Japan) or 5% skimmed milk were used for blocking. Primary antibodies for ALKBH5 (1:1000 dilution, HPA007196; Atlas Antibodies), FTO (1:1000 dilution, Ab124892; Abcam), IGF2BP1 (1:1000 dilution, 22803-1-AP; Proteintech), IGF2BP2 (1:1000 dilution, 11601-1-AP; Proteintech), IGF2BP3 (1:2000 dilution, 14642-1-AP; Proteintech), YTHDF2 (1:400, Ab170118, Abcam), TIMP3 (1:3000 dilution, Ab39184; Abcam), p21 (1:1000 dilution, A1483; ABclonal, Woburn, MA, USA), E2F1 (1:500 dilution, A2067; ABclonal), CCNG2 (0.2μg/mL, Ab251826; Abcam), p53 (1:200

dilution, Sc-126; SANTA CRUZ BIO TECHNOLOGY, Dallas, TX, USA), and GAPDH (1:1000 dilution, Ab8245; Abcam) were incubated for overnight at 4□. Secondary antibodies for rabbit (1:20000 dilution, NA9340; GE healthcare Life science) or mouse (1:20000 dilution, NA9310; GE Healthcare Life Science) were incubated at room temperature with 1%–5% skimmed milk for 1 h. Enhanced chemiluminescence (Pierce ECL Plus Substrate or West Atto Ultimate Sensitivity Substrate, Thermo Fisher Scientific) was used to visualize the protein bands using ChemiDocTouch (Bio-Rad).

Cell viability assay

Cells were seeded into 96-well plates with 3000 cells per well after 48 h of knockdown or overexpression. Cell proliferation was monitored using Cell Counting Kit-8 (CCK-8; Dojindo, Kumamoto, Japan) according to the manufacturer's protocol. Thereafter, the cells were incubated with 10% CCK-8 for 1 h, followed by absorbance assessment at 450 nm in each well via spectrophotometry (Synergy HT, BioTek, Winooski, VT, USA) every 24 h.

Transwell migration assay

Cell migration was evaluated using a 24-well plate with cell culture inserts (353097, Falcon, Mexico City, Mexico) containing a filter with 8 μm-diameter pores. Briefly, after serum starvation for 24 h with 0.1% FBS-containing RPMI1640 medium, 1×10^5 cells resuspended in 500 μL of RPMI1640 medium (Gibco) were seeded into the upper chamber, after which RPMI1640 medium containing 10% FBS was placed in the lower compartment of the chamber. After incubation for 16 h, the upper surface of the membrane was wiped with a cotton-tipped applicator to remove nonmigrating cells, whereas the migrating cells on the lower surface were fixed with cold methanol and stained with 0.5% crystal violet. Migrating cells were automatically counted in three random microscopic fields using the Hybrid Cell Count software (BZ-□ Analyzer, Keyence, Osaka, Japan).

Wound-healing assays

To assess cell migration, 2×10^5 cells were seeded into 6-well plates. Thereafter, cells were incubated in 5% CO_2 at 37□ for 48□h and an additional 24 h with 0.1% FBS-containing RPMI1640 medium. A wound was scratched into the cells using a 200-μL plastic tip and washed with PBS (−). The cells were then incubated in RPMI1640 containing 10% FBS. The relative distance of the scratches was observed

under an optical microscope (IX53, Olympus, Tokyo, Japan) at 3–6 time points after wounding and assessed using the Image J software.

Cell cycle assay and apoptosis assay

Cell Cycle Assay Solution Blue (C549, Dojindo) was used to measure the cell cycle according to the manufacturer's instructions. Briefly, treated cells were synchronized at the G1 phase through serum starvation with 0.1% FBS-containing medium for 48 h. At 24 h after the release of serum starvation, the treated cells were collected, washed with PBS (−), and incubated with 5 μL cell cycle assay solution for 15 min at 37□. Thereafter, DNA content was determined based on staining intensity using a Gallios flow cytometer (Beckman Coulter, Miami, FL, USA). The annexin V-FITC Apoptosis Detection Kit (15342-54 Nacalai) was used to detect apoptosis by measuring annexin V and propidium iodide (PI)-positive cells following the manufacturer's instructions. Briefly, cells were incubated for 96 h after siRNA transfection. To induce apoptosis, the cells were exposed to either 7.5 μM of gefitinib (078-06561, FUJIFILM) or 10 μM of cisplatin (P4394, Sigma-Aldrich) alone for 48 h after siRNA transfection. The treated cells were collected, washed with PBS (−), and incubated with 5 μL of annexin V-FITC solution and 5 μL of PI solution for 15 min. Thereafter, apoptotic cells were determined

using a Gallios flow cytometer. Results were analyzed using the FlowJo software (Becton, Dickinson, Franklin Lakes, NJ, USA), after which the extent of apoptosis and cell cycle distribution were determined.

RNA stability assay

Cancer cells were incubated for 48 h after siRNA transfection. Cells were treated with actinomycin D at a final concentration of 5 μg/mL. Total RNA was extracted at 0, 2, 4, and 6 h after adding actinomycin D. The remaining CDKN1A and TIMP3 mRNA was measured through quantitative real-time PCR and normalized to RPL32 mRNA, which has a half-life of 25 h.

Quantitative analysis of global m^6A levels using liquid chromatography–mass spectrometry/mass spectrometry (LC–MS/MS)

PolyA-enriched RNA was extracted using PolyATract mRNA isolation systems (#Z5310 Promega, Madison, WI, USA) according to the manufacturer's instructions. PolyA-enriched RNA concentration was calculated using Qubit 2.0. The polyA-enriched RNA was enzymatically hydrolyzed using 8-OHdG Assay Preparation Reagent Set (292-67801, FUJIFILM Wako Pure Chemical Corporation, Tokyo, Japan).

Technically, 100 ng of polyA-enriched RNA was digested using 5.7 μL of acetic acid buffer and 3 μL of Nuclease P1 included in the 45-μL sample containing nuclease-free water at 37□ for 30 min, followed by incubation with 6 μL of Tris Buffer and 0.3 μL of alkaline phosphatase at 37□ for 30 min. After digestion, the sample was centrifuged at 14,000 *g* and 4□ for 20 min using a Nanosep 3K Omega centrifugal device (Pall Corporation, Port Washington, NY, USA) according to a previously published method (46).

As an internal standard, N^6-methyladenosine-d3 (m^6A-d3; M275897, Toronto Research Chemicals, Toronto, Canada), which is a stable isotope of N^6-methyladenosine labeled with three deuterium atoms on the N^6-methyl group, was added to the nucleosides obtained via digestion of polyA-enriched RNA. These nucleosides were separated using an Acquity UPLC HSS T3 column (2.1 mm × 100 mm; Waters, Milford, CT, USA) with 0.1% (vol./vol.) formic acid in water as mobile phase A and methanol as mobile phase B at a flow rate of 200 μL/min in a linear gradient elution of 5%–60% B from 0 to 7 min. Standard compounds of adenosine (A; A9251, Sigma-Aldrich), N^6-methyladenosine (m^6A; A170736, Sigma-Aldrich), and m^6A-d3 were used to confirm the nucleoside-to-base ion mass transitions of 268.1–136.4 (A), 282.2–150.2 (m^6A), and 285.2–153.2 (m^6A-d3). Peak areas of A, m^6A, and m^6A-d3 in the nucleosides digested

323 from polyA-enriched RNA were calculated using the column retention time of the
324 standard compounds using Analyst 1.6.1 software (AB SCIEX, Foster City, CA, USA).
325 The m^6A level was quantified as the ratio of m^6A to A or m^6A-d3 based on the
326 calibrated concentrations.
327
328 **Microarray analysis of differentially expressed genes**
329 Total RNA was extracted from ALKBH5-knockdown or control PC9 cells 96 h after
330 transfection. RNA samples were used for global gene expression profiling on human
331 Clariom S Assay microarrays (Thermo Fisher Scientific, Wilmington, DE, USA), which
332 include 24351 genes. All microarray analyses were entrusted to Filgen Inc. (Aichi,
333 Japan). A total RNA quality control check was performed using a NanoDrop ND-1000
334 (Thermo Scientific) and an Agilent 2100 Bioanalyzer. Using the Gene Chip TM WT
335 PLUS Reagent Kit, fragmented and labeled cDNA samples were prepared from 250 ng
336 of total RNA according to the manufacturer's instructions (Gene Chip TM WT PLUS
337 Reagent Kit User Manual). Thereafter, 100 μL of hybridization solution was prepared
338 using 73 μL of Hybridization Master Mix and 2.3 μg of fragmented and labeled cDNA.
339 The array was incubated using the Gene Chip TM Hybridization Oven 645 at 45□ for
340 16 h (60 rpm). The array was cleaned using the Gene Chip TM Fluidics Station 450 and

scanned using the Gene Chip TM Scanner 3000 7G according to the manufacturer's instructions [Gene Chip TM Command Console (AGCC) 4.0 User Manual]. The Microarray Data Analysis Tool version 3.2 (Filgen, Aichi, Japan) was used for data normalization and subsequent processing. Differentially expressed mRNAs were identified using a set cutoff (fold change > 1.5 or < 0.67; $P < 0.01$). Gene set enrichment analysis (GSEA) was performed to examine the gene sets regulated by ALKBH5 knockdown (http:/software.broadinstitute.org/gsea/omdex.jsp). For analysis, the false discovery rate (FDR) based on gene set permutation was used. Microarray data has been deposited in the Gene Expression Omnibus (GEO) at the National Center for Biotechnology Information (NCBI) (accession number GSE165453).

Epitranscriptomic microarray analysis

Unfragmented total RNA was extracted from ALKBH5-knockdown or control PC9 cells at 96 h after transfection and quantified using the NanoDrop ND-1000. RNA samples were used for global m^6A expression profiling on an Arraystar Human mRNA&lncRNA Epitranscriptomic Microarray (8 × 60 K; Arraystar), which includes 44,122 protein-coding mRNAs and 12,496 long noncoding RNAs. Microarray analyses were entrusted to Arraystar Inc. (Rockville, MD, USA). Sample preparation and microarray

hybridization were performed based on Arraystar's standard protocols. Briefly, total RNAs were immunoprecipitated with an anti-m^{6}A antibody (Synaptic Systems, 202003). The "immunoprecipitated (IP)" and "supernatant (Sup)" RNAs were labeled with Cy5 and Cy3, respectively, as cRNAs in separate reactions using the Arraystar Super RNA Labeling Kit. The cRNAs were combined and hybridized onto Arraystar Human mRNA&lncRNA Epitranscriptomic Microarray (8 × 60 K, Arraystar). After washing the slides, the arrays were scanned in two-color channels using an Agilent Scanner G2505C. Agilent Feature Extraction software (version 11.0.1.1) was used to analyze acquired array images. Raw intensities of IP (Cy5-labeled) and Sup (Cy3-labeled) were normalized with an average of log2-scaled Spike-in RNA intensities. The "m^{6}A methylation level" was calculated to determine the percentage of modification based on the IP (Cy5-labeled) and Sup (Cy3-labeled) normalized intensities. "m^{6}A quantity" was calculated to determine the amount of m^{6}A methylation based on the IP (Cy5-labeled) normalized intensities. Differentially m^{6}A-methylated RNAs between both comparison groups were identified by filtering with a fold change of >1.5 or <0.67 ($P < 0.01$) through the unpaired *t*-test. Microarray data had been deposited in the GEO at the NCBI (accession number GSE165454).

qPCR for methylated RNA immunoprecipitation (MeRIP) with m^{6}A antibody

ALKBH5-knockdown or control lung cancer cells were used for methylated RNA immunoprecipitation assay. The Magna MeRIP m^{6}A kit (catalog no.17-10499, Millipore, Burlington, MA, USA) was used according to the manufacturer's protocol. Briefly, the polyA-enriched RNA was fragmented into 100–200 nucleotides incubated with RNA fragmentation buffer for 55 s (CS220011, Millipore). The size of polyA-enriched RNA fragments was optimized using the Agilent 4200 TapeStation (Agilent technologies, Santa Clara, CA, USA). We used 0.5 μg of fragmented polyA-enriched RNA as input control and 5 μg of fragmented polyA-enriched RNA for m^{6}A mRNA immunoprecipitation, followed by incubation with m^{6}A antibody (MABE1006, Millipore)- or mouse IgG-conjugated Protein A/G Magnetic Beads in 500 μL 1× IP buffer supplemented with RNase inhibitors at 4□ overnight. Methylated RNAs were immunoprecipitated with beads, eluted via competition with free m^{6}A, and purified using the RNeasy kit (Qiagen). Moreover, modification of m^{6}A toward particular genes was determined using qPCR analysis with specific primers [primers for the positive control region (stop codon, EEF1A1+) or NC region (exon 5, EEF1A1−) of human EEF1A1 was included in the Magna MeRIP m6A kit]. To design primers for MeRIP qPCR, m^{6}A sites of specific genes were predicted using the sequence-based RNA

adenosine methylation site predictor algorithm (http://www.cuilab.cn/sramp) (47). We focused on the potential m^6A sites in the 3′ UTRs near the stop codon and designed primers to ensure that the target sequences were present in these sites with a limited length of 120 nt. Self-designed primers for MeRIP qPCR are listed in Table S1.

Statistical analysis

Discrete variables were expressed as numbers (percentages), whereas continuous variables were expressed as means ± standard deviations (SDs) unless otherwise specified. The Mann–Whitney *U* test was used to compare continuous individual samples, whereas Student's *t*-test was applied to compare continuous experimental data. Fisher's exact test for independence was used to compare categorical data between groups. The Wilcoxon matched-pairs signed-rank test was used to compare two corresponding groups. Spearman's correlation coefficient was used for correlation analysis. Kaplan–Meier curves with log-rank tests were used to analyze survival. Accordingly, OS was defined as the duration from baseline to the date of death, whereas recurrence-free survival (RFS) was defined as the duration from baseline to the recurrence date. Univariate and multivariate Cox proportional hazards models were applied to generate hazard ratios (HRs) for death while adjusting for other potential

413 confounding factors. Cell proliferation and RNA stability assays were analyzed using
414 two-way analysis of variance. Statistical analyses were performed using GraphPad
415 Prism Version 8 (GraphPad Software, San Diego, CA, USA) and EZR software
416 (Saitama Medical Center, Jichi Medical University, Saitama, Japan), with *P* values of
417 <0.05 indicating statistical significance.
418

419 **Results**

420 **High ALKBH5 expression was associated with a worse prognosis in patients with**
421 **NSCLC**

422 To investigate the impact of ALKBH5 and FTO in NSCLC, we examined the mRNA
423 expression levels of ALKBH5 and FTO in non-cancerous lung tissues and NSCLC
424 tissues using TCGA data. Accordingly, our results showed no significant difference in
425 ALKBH5 mRNA expression between non-cancerous and cancerous tissues. By contrast,
426 our findings showed that NSCLC had a significantly lower FTO mRNA expression than
427 non-cancerous tissues (Fig. 1A). We subsequently investigated the protein expression
428 levels of ALKBH5 and FTO in non-cancerous lung alveolar tissue and corresponding
429 NSCLC tissues using TMA of patient samples. Furthermore, our results showed that
430 cancerous tissues had significantly higher H-scores for ALKBH5 and FTO than

non-cancerous tissues (Fig. 1B). ALKBH5 and FTO expression were evaluated in immortalized bronchial epithelial cells (BEAS2B) and lung cancer cell lines. Consequently, qPCR analysis demonstrated that ALKBH5 mRNA expression was higher in lung cancer cell lines except for LC-2/ad and RERF-LC–MS, whereas FTO mRNA expression was lower in lung cancer cell lines except for HLC-1, ABC1, and PC3 (Fig. 1C). Western blot analysis demonstrated that ALKBH5 was endogenously expressed in all lung cancer cell lines and FTO was expressed in almost all lung cancer cell lines except HLC-1 (Fig. 1D). IHC analysis showed that ALKBH5 and FTO were mainly localized in the nucleus of the cells (Fig. 1E). Furthermore, immunofluorescence analysis showed that ALKBH5 was localized in the nucleus of PC9 cells overexpressing ALKBH5 (Fig. 1F). We analyzed the clinical characteristics of 627 NSCLC cases used in IHC of TMA in the context of ALKBH5 or FTO expression in tumors of the HUSM cohort (Table S2). The median age was 68 (range, 23–88) years; 430 (68.6%) patients were male and 184 (29.3%) had never smoked. The tumors were histologically classified as adenocarcinoma (n = 413, 65.9%), squamous cell carcinoma (n = 170, 27.1%), or other histological types (n = 44, 7.0%). A total of 395 (63.0%) patients had stage I disease, whereas 127 (20.3%) cases had EGFR mutations. Postoperative adjuvant chemotherapy was prescribed to 258 (41.1%) patients. The median H-score

449 values for ALKBH5 and FTO expression were 110 (0–225, range) and 65 (0–281),
450 respectively, with high ALKBH5 protein expression being correlated with high FTO
451 protein expression (r = 0.41) (Fig. S1A). Based on the median value, cases were divided
452 into “high” and “low” expression groups, after which their association with clinical data
453 as well as prognostic significance was examined. Lymph node metastasis, chemotherapy,
454 and EGFR status significantly differed depending on ALKBH5 expression, whereas
455 tumor status, lymph node metastasis, pathological stage, chemotherapy, and EGFR
456 status significantly differed depending on FTO expression. Kaplan–Meier curves
457 showed that patients with high ALKBH5 expression had significantly worse survival
458 than those with low ALKBH5 expression (Fig. 1G: log-rank p = 0.0009 for OS; Fig.
459 S1B: log-rank p = 0.0008 for RFS). Conversely, Kaplan–Meier curves showed no
460 significant difference in survival between the low and high FTO expression groups (Fig.
461 1G: log-rank p = 0.20 for OS, Fig. S1C: log-rank p = 0.07 for RFS). Univariate analysis
462 revealed high ALKBH5 expression as a predictor of unfavorable OS (HR, 1.675; 95%
463 CI, 1.230–2.521). Moreover, multivariate analysis of age, sex, smoking status, histology,
464 pathological stage, and ALKBH5 expression revealed that ALKBH5 expression was an
465 independent prognostic factor associated with unfavorable OS (HR, 1.468; 95% CI,
466 1.039–2.073) (Table S3). To validate the prognostic value of ALKBH5 and FTO in

other cohorts of patients with NSCLC, the lung cancer database in the Kaplan–Meier plotter was used. Accordingly, Kaplan–Meier curves showed that patients with high ALKBH5 expression had a significantly worse survival than those with low ALKBH5 expression (Fig. S1D: log-rank $p = 0.014$ for OS). In contrast, Kaplan–Meier curves showed that patients with high FTO expression had significantly favorable survival compared with those with low FTO expression (log-rank $p < 0.0001$ for OS) (Fig. S1E). These observations suggested that ALKBH5 played a critical role in the poor prognosis of patients with NSCLC.

ALKBH5 knockdown suppressed cell proliferation in NSCLC

To investigate the impact of ALKBH5 and FTO deficiency in lung cancer cell function, ALKBH5 and FTO were knocked down in PC9 and A549 cells using small interfering RNA (siRNA). Based on knockdown efficacy, ALKBH5 siRNA no. 1 (siALKBH5#1) and siRNA no. 3 (siALKBH5#3) and FTO siRNA no.1 (siFTO#1) and siRNA no. 3 (siFTO#3) were used in subsequent knockdown experiments (Fig. 2A, 2B, and S2A). ALKBH5 knockdown significantly suppressed the proliferation of PC9 and A549 cells (Fig. 2C). By contrast, FTO knockdown showed no significant suppressive effects on the proliferation of PC9 and A549 cells (Fig. 2D). Thereafter, we assessed migration

485 abilities in ALKBH5-knockdown cells. Accordingly, the transwell migration assay
486 showed no significant reduction in the migratory PC9 and A549 cells (Fig. 2E).
487 Moreover, the wound-healing assay showed that ALKBH5 knockdown promoted no
488 significant reduction in the migration ability of PC9 and A549 cells (Fig. 2F and 2G).
489 Together with the prognostic value of ALKBH5 in NSCLC, these observations
490 suggested that ALKBH5 played a cancer-promoting role by regulating cell proliferation.
491 To subsequently examine the mechanism by which ALKBH5 knockdown
492 suppressed cell proliferation, cell cycle, and apoptosis analyses were performed using
493 flow cytometry. Accordingly, ALKBH5 knockdown significantly increased the number
494 of PC9 cells in the G1 phase and reduced the number of PC9 cells in the G2/M phase
495 with a consistent result of two different sequences of siRNAs (Fig.3A and 3B). On the
496 other hand, the number of A549 cells in the G1 phase did not show significant
497 differences by ALKBH5 knockdown with siALKBH5#1 and significantly increased by
498 ALKBH5 knockdown with siALKBH5#3. The number of A549 cells in the G2/M phase
499 did not show significant differences by ALKBH5 knockdown with a consistent result of
500 two different sequences of siRNAs (Fig. 3C, 3D). ALKBH5 knockdown increased the
501 number of apoptotic PC9 cells (Fig. 3E and 3F). Furthermore, under drug-induced
502 apoptosis via cisplatin and gefitinib administration, ALKBH5 knockdown also

503 increased the number of apoptotic PC9 cells (Fig. 3G and 3H). ALKBH5 knockdown
504 also increased the number of apoptotic A549 cells (Fig. 3I and 3J). Moreover, ALKBH5
505 knockdown increased the number of apoptotic A549 cells with cisplatin (Fig. 3K and
506 3L). Overall, the aforementioned data showed that ALKBH5 knockdown suppressed
507 cell proliferation through G1 phase arrest and/or apoptosis induction in NSCLC cell
508 lines.
509
510 **ALKBH5 overexpression promoted cell proliferation in immortalized cells**
511 To analyze whether ALKBH5 overexpression in immortalized cells promoted malignant
512 changes in cell function, BEAS2B and HEK293 cells, which are immortalized cells,
513 were infected with a doxycycline-inducible vector, pRetroX-TetOne puro-ALKBH5.
514 ALKBH5 overexpression was confirmed in HEK293 and BEAS2B cells (Fig. 4A) and
515 significantly enhanced HEK293 and BEAS2B cell proliferation (Fig. 4B and 4C). In
516 contrast, ALKBH5 overexpression showed no significant effects on the migration
517 ability of HEK293 (Fig. 4D and 4E) and BEAS2B cells (Fig. 4F and 4G). The
518 aforementioned results provided further evidence that ALKBH5 played a
519 cancer-promoting role by regulating cell proliferation.
520

521 **ALKBH5 altered the abundance of m^{6}A modification in polyA-enriched RNA**

522 To assess the amount of m^{6}A in cells, a quantitative evaluation of m^{6}A was performed
523 via LC–MS/MS using polyA-enriched RNA extracted from PC9 cells with altered
524 ALKBH5 gene expression (Fig. 5A). We investigated the technical variability that
525 occurs when adenosine and *N*^{6}-methyladenosine-d3 (m^{6}A-d3) are used as internal
526 standards. Although both adenosine (A) and m^{6}A-d3 showed a strong positive
527 correlation with m^{6}A ($r = 0.92$ and $r = 0.90$), the measurement with m^{6}A-d3 as the
528 internal standard showed less technical variability than that with A as the internal
529 standard (Fig. S3A–C). Hence, we used m^{6}A-d3 as the internal control for subsequent
530 experiments. ALKBH5 knockdown increased m^{6}A modification in PC9 and A549 cells
531 (Fig. 5B and 5C), whereas ALKBH5 overexpression reduced m^{6}A modification in a
532 doxycycline concentration-dependent manner in PC9 cells (Fig. 5D, S3D, and S3E).
533 Moreover, ALKBH5 overexpression reduced m^{6}A modification regardless of the time
534 that had elapsed after doxycycline addition (Fig. 5E). Furthermore, ALKBH5
535 overexpression reduced m^{6}A modification in BEAS2B and HEK293 cells (Fig. 5F). The
536 aforementioned results presented evidence suggesting that ALKBH5 alters the global
537 m^{6}A abundance in cells.
538

ALKBH5 regulated the expression of cell proliferation-related genes

An expression microarray analysis was herein performed to investigate gene expression profiles in ALKBH5-knockdown PC9 cells with two different sequences of siRNA (ALKBH5#1 and ALKBH5#3). Differentially expressed genes (DEGs) were defined as those with a fold change of >1.5 or <0.67 ($P < 0.01$). A total of 697 DEGs were detected for ALKBH5#1 comprising 392 upregulated and 305 downregulated genes (Fig. 6A), whereas 1394 DEGs were detected for ALKBH5#3 comprising 803 upregulated and 591 downregulated genes (Fig. 6B). Moreover, 82 upregulated genes (Table S4) and 47 downregulated genes (Table S5) overlapped between ALKBH5#1 and ALKBH5#3 (Fig. 6C). Except for ALKBH5, genes associated with m^6A modification described in a previous review (48) were not included in the overlapped DEGs (Table S6). GSEA with the hallmark gene set revealed that the PC9 cells transfected with siALKBH5#1 and siALKBH5#3 had a more enriched expression of genes involved in cell cycle, such as MYC_TARGETS_V2, P53_PATHWAY, and G2/M_CHECKPOINT, than those transfected with siNC (Fig. S4A and S4B). We selected 10 DEGs associated with cell proliferation or apoptosis based on their description in the NCBI gene summary (49-54) or by referring to previous literature (55-58) and confirmed the upregulation of E2F1, GADD45A, TIMP3, and CDKN1A and downregulation of CASP14 and CCNG2 by

qPCR (Fig. 6D). The aforementioned results revealed that ALKBH5 regulated the expression of genes associated with cell proliferation.

ALKBH5 altered the abundance of m^{6}A in the 3′ UTR and regulated protein expression of target genes

We performed m^{6}A-specific methylated RNA immunoprecipitation microarray analysis in PC9 cells on an Arraystar Human mRNA&lncRNA Epitranscriptomic Microarray to comprehensively examine whether differentially regulated genes were associated with m^{6}A modification using unfragmented total RNA. The median methylation level in unfragmented total RNA was 50.4% (6.8%–94.5%) (Fig. S5A). A positive correlation was observed between the methylation level in unfragmented total RNA and the RNA length of each transcript (r = 0.35) (Fig. S5B). Moreover, a negative correlation was noted between the rate at which ALKBH5 knockdown increased m^{6}A modification (methylation level in siALKBH5 − methylation level in siNC) and methylation level at baseline (methylation level in siNC) (r = −0.35) (Fig. S5C). The volcano plot showed that 1 RNA was hypermethylated by ALKBH5#1 knockdown (fold change > 1.5, P < 0.01) (Fig. S5D), whereas 28 RNAs were hypermethylated by ALKBH5#3 knockdown (fold change > 1.5; P < 0.01) (Fig. S5E). No hypermethylated genes overlapped

575 between ALKBH5#1 and ALKBH5#3 knockdown with a fold change threshold of >1.5
576 ($P < 0.01$) (Fig. S5F). GSEA showed no common hallmark gene set with an FDR
577 q-value of < 0.25 for PC9 cells transfected with siALKBH5#1 and siALKBH5#3
578 compared with the control group (Fig. S5G).

579 Considering that the m^6A levels of unfragmented RNAs regulated by ALKBH5
580 are affected by the baseline RNA length and endogenous m6A level, we performed
581 methylated RNA immunoprecipitation (MeRIP) with m^6A antibody using fragmented
582 polyA-enriched RNA in ALKBH5-knockdown PC9 cells to investigate focal m^6A
583 alterations in the mRNA. The fragmentation conditions were optimized (Fig. S6A), and
584 the m^6A changes in the positive and NC were confirmed through qPCR using the
585 primers included in the Magna MeRIP m^6A Kit (Millipore) (Fig.S6B). To verify the
586 accuracy of the MeRIP experiment, we selected MFAP5 out of the 11 hypermethylated
587 genes (>1.5 fold change and $P < 0.05$) in the human mRNA&lncRNA Epitranscriptomic
588 Microarray (Table S7) and analyzed the m^6A target site via qPCR. Specific primers
589 were designed for the predicted m^6A-harboring regions, and MeRIP qPCR confirmed
590 that ALKBH5 knockdown increased m^6A levels in the 3′ UTR of MFAP5 (Fig. S6C).
591 Thereafter, MeRIP qPCR was performed in six DEGs verified using qPCR with
592 ALKBH5-knockdown PC9 cells. Our results showed increased m^6A levels in the 3′

593 UTRs of CDKN1A, TIMP3, E2F1, and CCNG2 in ALKBH5-knockdown PC9 cells
594 (Fig. 6E–6G). ALKBH5 knockdown with two different sequences of siRNAs also
595 increased the m^6A level in the 5'UTR of CDKN1A (Fig. 6F). The aforementioned
596 results of the MeRIP qPCR suggest that ALKBH5 targeted the 3′ UTRs of m^6A in these
597 four transcripts (Fig. 7A).

598 Next, the protein expression levels of the potential target transcript of ALKBH5
599 were quantified by western blot analysis. Accordingly, our results showed that
600 CDKN1A (p21) expression increased independent of p53 in ALKBH5-knockdown PC9
601 cells, whereas TIMP3 expression increased in ALKBH5-knockdown A549 cells (Fig.
602 7B).

603 To investigate the effect of both CDKN1A in PC9 and TIMP3 in A549 on cell
604 proliferation in ALKBH5-deficient lung cancer cell lines, we confirmed the reduced
605 expression using siRNA (Fig. 7C, 7D, S7A, and S7B). The knockdown of CDKN1A
606 partly rescues the decreased cell proliferation in ALKBH5-deficient PC9 cells (Fig. 7E).
607 The knockdown of TIMP3 also partly rescues the decreased cell proliferation in
608 ALKBH5-deficient A549 cells (Fig. 7F). These results suggest that CDKN1A and
609 TIMP3 are important targets for cell proliferation and are required for cell number
610 reduction by repression of ALKBH5.

Additionally, we evaluated the expression of ALKBH5 target mRNAs CDKN1A and TIMP3 in lung cancer using the TCGA dataset. Accordingly, cancerous tissues (high ALKBH5 expression) had lower CDKN1A and TIMP3 expression than noncancerous tissue (low ALKBH5 expression; Fig. S7C and S7D). The results were consistent with the experimental results of CDKN1A and TIMP3 knockdown described above.

IGF2BPs were required for ALKBH5 regulation of target mRNA expression via stabilization of mRNA and affected cell proliferation

IGF2BP1, IGF2BP2, IGF2BP3 (IGF2BPs), and YTHDF2 are well-known m^6A-recognizing RNA-binding proteins and readers of m^6A that have been known to stabilize or destabilize mRNA. The expression of proteins of IGF2BPs in a series of cell lines was analyzed by western blotting, and the results showed differences in their expression in lung cancer cells and immortalized bronchial epithelial cells according to the cell lines (Fig.8A).

Thereafter, ALKBH5 and IGF2BPs were knocked down with siRNA to investigate the association between ALKBH5 and IGF2BPs and the expression of CDKN1A (p21) or TIMP3 (Fig. S8A–D). Western blot analysis revealed that IGF2BPs

knockdown sufficiently reduced the expression of IGF2BPs (Fig. 8B), although some of them appeared to be weakly expressed as shown in Figure 8A. Accordingly, ALKBH5 knockdown increased the mRNA expressions of CDKN1A in PC9 cells and TIMP3 in A549 cells. The knockdown of IGF2BPs alone did not significantly change the expression of CDKN1A and TIMP3 (Fig. S8E), but that of both ALKBH5 and IGF2BPs offset the increased expression of CDKN1A and TIMP3 (Fig. 8C). We further analyzed the protein expression of YTHDF2 in lung cancer cell lines (Fig. 8D) and conducted transfection of siRNA for YTHDF2 as previously described (59), which confirmed that upregulated expression of CDKN1A by ALKBH5 knockdown was increased by YTHDF2 knockdown in PC9, which suggested that m^6A of CDKN1A may be affected by both IGF2BPs and YTHDF2 reversibly (Fig. 8E and S8F). Actinomycin D assay showed that ALKBH5 knockdown stabilized CDKN1A mRNA in PC9 cells, and this stabilization was offset by the knockdown of IGF2BPs. ALKBH5 knockdown also stabilized TIMP3 mRNA in A549 cells, although not statistically significant, and this stabilization was decreased by IGF2BP3 knockdown (Fig. 8F). These results suggest that these alterations in mRNA expression were offset by a double knockdown of both ALKBH5 and one of the IGF2BPs, and the decline of mRNAs was, at least partly, owing to the destabilization of these mRNAs by one of the IGF2BPs.

Considering that the interaction between ALKBH5 and IGF2BPs was found to regulate the expression of genes associated with cell proliferation, cell proliferation assays were conducted using ALKBH5- and IGF2BPs-knockdown cells. The knockdown of IGF2BPs did not cause a significant change in cell proliferation in PC9 cells, but the knockdown of IGF2BPs decreased cell proliferation in A549 cells (Fig. S8G). Notably, ALKBH5 knockdown reduced cell proliferation in PC9 and A549 cells and this reduction of cell proliferation was offset by IGF2BPs knockdown (Fig. 8G). These results suggest that the increased effect of cell proliferation upon simultaneous knockdown of IGF2BPs and ALKBH5 cannot be explained by the effect of IGF2BPs alone. Overall, our results support the hypothesis that IGF2BPs are required for ALKBH5 regulation of target mRNA expression and cell proliferation.

Discussion

The current study revealed that ALKBH5 promoted poor survival and cell proliferation in patients with NSCLC. Mechanistically, ALKBH5 knockdown had been found to increase the expression of CDKN1A (p21) and TIMP3 by altering mRNA stability in PC9 and A549 cells via m^6A change. Moreover, these changes in mRNA stability were counteracted by IGF2BPs knockdown. The aforementioned results

665 suggest that the recognition of target transcripts by IGF2BPs stabilizes the mRNA of
666 CDKN1A (p21) or TIMP3 and subsequently increases their expressions, thereby
667 regulating cell proliferation, cell cycle, and apoptosis in lung cancer cell lines.
668 Over the last decade, considerable progress has been made on research
669 regarding the molecular mechanism for m^6A-mediated carcinogenesis of ALKBH5.
670 Nevertheless, previous studies on ALKBH5 have shown conflicting results regarding
671 the carcinogenic mechanisms of ALKBH5 across several cancers (28-36). Several
672 previous studies have reported contradictory results regarding ALKBH5, suggesting that
673 it acts as either an oncogenic factor or a tumor suppressor in NSCLC (40-42). The
674 current study concluded that ALKBH5 exerted cancer-promoting effects in NSCLC by
675 suppressing CDKN1A (p21) or TIMP3. On the other hand, although both ALKBH5 and
676 FTO are classified as m^6A demethylases, there was a discrepancy in survival between
677 ALKBH5 and FTO (Fig. 1G). Indeed, there was a trend toward a worse prognosis in the
678 FTO high-expression group, but the difference was not significant (Fig. 1G).
679 Furthermore, the knockdown of FTO did not suppress the proliferation of lung cancer
680 cells, but the knockdown of ALKBH5 inhibited it. Thus, ALKBH5 appears to have a
681 more effective impact on carcinogenesis. Certainly, our immunostaining results also
682 revealed a weak correlation between ALKBH5 and FTO expression, but some cases had

683 different intensities of expression among proteins (Fig. S1A). A possible background
684 mechanism is that each eraser protein may regulate a different target demethylated gene.
685 Independent changes of ALKBH5 and FTO expression would allow for complex
686 regulation of downstream gene expression via m^6A.

687 CDKN1A (p21) functions as a cell growth suppressor by inhibiting cell cycle
688 progression. Multiple transcription factors, ubiquitin ligases, and protein kinases
689 regulate the transcription, stability, and cellular localization of CDKN1A (p21) (60). A
690 previous study showed that ALKBH5 knockdown increased m^6A modification and
691 mRNA stability of CDKN1A, which subsequently increased p21 protein expression and
692 acted as a tumor suppressor in esophageal cancer (32). Similarly, our findings showed
693 that ALKBH5 knockdown in PC9 cells acted as a tumor suppressor by the upregulation
694 of CDKN1A (p21) via m^6A alteration. We also showed that p21 upregulation was
695 p53-independent and reduced cell proliferation in ALKBH5-deficient PC9 cells was
696 rescued by CDKN1A knockdown, which indirectly reinforced our finding that
697 CDKN1A (p21) upregulation was critical for an m^6A-mediated response. Our results
698 further indicated a novel mechanism wherein changes in CDKN1A expression via
699 ALKBH5 knockdown were rescued by IGF2BPs knockdown, which supports our
700 finding that alterations in CDKN1A (p21) expression were mediated by m^6A.

The current study identified TIMP3 as another important target molecule downstream of ALKBH5. A previous study showed TIMP3 had several anticancer properties, including apoptosis induction and antiproliferative, antiangiogenic, and antimetastatic activities. The expression of TIMP3 is regulated by transcription factors and histone acetylation (61). Several studies have shown that TIMP3 acts as a tumor suppressor in lung cancer (62, 63). Indeed, TIMP3 knockdown increased cell proliferation in A549 cells and rescued cell proliferation in ALKBH5-deficient A549 cells. Moreover, a previous report using A549 cell lines showed that ALKBH5 knockdown increases TIMP3 mRNA stability and TIMP3 expression via m^6A modification (41). Similarly, the current study also confirmed that ALKBH5 knockdown increased mRNA stability, which increased TIMP3 protein expression and acted as a tumor suppressor in A549 cells. Furthermore, our experimental data for the first time showed that the ALKBH5 knockdown-induced increase in TIMP3 was rescued by IGF2BPs, strongly suggesting that alterations in TIMP3 expression were mediated by m^6A.

IGF2BPs are known as m^6A-recognizing RNA-binding proteins that stabilize m^6A-containing RNA. Previous studies have reported that IGF2BPs have oncogenic properties. Studies on lung cancer have associated IGF2BPs with cancer progression

719 and poor prognosis (64-69). Notably, a previous report showed that ALKBH5-mediated
720 m^6A modification of LY6/PLAUR Domain Containing 1 (LYPD1) is recognized by
721 IGF2BP1 and enhances the stability of LYPD1 mRNA in hepatocellular carcinoma (35).
722 Moreover, recent RNA-binding protein immunoprecipitation-sequencing analysis using
723 HEK293T showed that the binding site of IGF2BPs is mainly distributed in the 3′ UTRs
724 and that the target of IGF2BPs preferentially binds to the consensus sequence of
725 UGGAC in the target mRNA (26). These findings support our experimental hypothesis
726 that IGF2BPs recognize the m^6A in the 3′ UTRs of CDKN1A or TIMP3 because
727 UGGAC is present within three locations in the 3′ UTRs of CDKN1A and two locations
728 in the 3′ UTRs of TIMP3. In addition, IGF2BPs regulate RNA expression by
729 recognizing m^6A to affect mRNA stability. Their binding sites for m^6A modification are
730 enriched in the 3'UTR. On the other hand, the distribution of binding peaks differs
731 somewhat depending on the subclass of IGF2BPs, and nearly 50% of the targets in each
732 IGF2BP subclass are different in the other subclass (26). Our findings also showed that
733 the expression of IGF2BPs significantly differed between cell lines. It is possible that
734 IGF2BP subclasses with different m^6A targets play a role in the more complex
735 regulation of the expression of various target genes by changing their expression levels
736 depending on cell types. As a result, although PC9 and A549 are both lung

adenocarcinoma cell lines, the protein expression of their target genes such as CDKN1A (p21) or CCNG2 may have been different (Fig. 7B).

In our epitranscriptomic microarray, site-specific changes in m^6A modification could not be determined since sample RNAs were not fragmented. Considering the correlation between RNA length and the ratio of m^6A-modified transcripts, the epitranscriptomic microarray analysis using unfragmented RNA does not allow the evaluation of multiple m^6A modifications occurring within a single transcript. As such, we conducted MeRIP q-PCR with fragmented RNAs to evaluate site-specific differential m^6A modification. Nevertheless, the epitranscriptomic microarray with unfragmented RNAs provided a holistic view of the degree of m^6A modification for each transcript, establishing a landscape for m^6A modification by ALKBH5 knockdown (Fig. S5A–E and S5G).

FTO inhibitors have been shown to suppress the progression of acute myeloid leukemia and glioblastoma *in vivo* (70, 71). In contrast, the antitumor effects of ALKBH5 inhibitors, which enhanced the efficacy of cancer immunotherapy, have only been confirmed in melanomas (72). Furthermore, several experimental facts have shown that ALKBH5 is associated with the malignant transformation of cancer (28-34), indicating that ALKBH5 inhibitors can be a target of tumor-agnostic therapy. However,

it should be noted that ALKBH5 inhibitors may cause unexpected side effects in unknown target genes given that ALKBH5 inhibition alters the m6A modification of numerous transcripts and the expression of several genes.

Although the current study provided abundant evidence to conclude the remarkable role of the m^6A-regulated ALKBH5 and IGF2BPs axis in NSCLC, several limitations warrant consideration. First, the possibility that off-target effects of siRNAs may have affected the results cannot be ruled out because the number of nonoverlapping DEGs was not small in the expression microarray results (Fig. 6C). To maximally eliminate the influence of the off-target effect, we used two different sequences of siRNA. Secondly, our epitranscriptomic microarray findings showed that ALKBH5-knockdown reduced m^6A methylation levels in approximately half of the transcripts. Although the detailed mechanism remains unclear, hypomethylation may occur when some of the m^6A-rich transcripts bind to YTHDF2 and YTHDC2, reducing the stability of RNA containing m^6A. Consequently, the m^6A-modified transcript then undergoes degradation over time. In other words, the target's transcript may also differ depending on the elapsed time after the perturbation of ALKBH5. However, the current study did not investigate the chronological alteration of the m^6A abundance of each transcript following ALKBH5 knockdown. Third, as mentioned earlier, CDKN1A and

773 TIMP3 are also regulated by transcription factors or miRNA, and we cannot deny the
774 possibility that mechanisms other than m^6A promoted changes in CDKN1A (p21) and
775 TIMP3 expression. Nonetheless, the finding that IGF2BPs knockdown rescued the
776 CDKN1A and TIMP3 expression supports our proposition that the changes in CDKN1A
777 (p21) and TIMP3 expression were mediated via m^6A.
778

779 **Conclusions**

780 The current study revealed that increased ALKBH5 expression was an independent
781 unfavorable prognostic factor in NSCLC. Moreover, upregulation of ALKBH5 in
782 NSCLC reduced m^6A modifications on the 3′ UTR of specific genes. The loss of m^6A
783 decreased the opportunity for recognition by IGF2BPs and destabilized the target
784 transcripts such as CDKN1A (p21) and TIMP3. Downregulation of CDKN1A (p21) and
785 TIMP3 induced cell cycle alteration and inhibited apoptosis. Our results suggest that the
786 ALKBH5–IGF2BPs axis promotes cell proliferation and tumorigenicity, which in turn
787 causes the unfavorable prognosis of NSCLC. Our findings provide a novel insight into
788 the pathophysiological mechanisms of m^6A epitranscriptomic modification in NSCLC
789 (Fig. 8H). Further *in vivo* studies are nonetheless required to determine whether
790 ALKBH5 inhibitors can be incorporated in the treatment of NSCLC in the near future.

List of abbreviations

m^{6}A: *N*^{6}-methyladenosine; NSCLC: non-small-cell lung cancer; MeRIP: Methylated RNA immunoprecipitation; CI: Confidence interval; HR: Hazard ratio; UTRs: 3′ untranslated regions; METTL3: methyltransferase-like 3; METTL14: Methyltransferase-like 14; WTAP: Wilms tumor 1-associated protein; RBM15: RNA-binding motif protein 15; FTO: fat mass and obesity-related protein, ALKBH5: AlkB homolog 5; YTHDC: YT521-B homology domain containing; HNRNPG: heterogeneous nuclear ribonucleoprotein G; YTHDF: YT521-B homology domain family; eIF3: eukaryotic initiation factor3; IGF2BP: insulin-like growth factor 2 mRNA-binding protein; m^{6}Am: *N*^{6},2′-*O*-dimethyladenosine; TMA: Tissue microarray; IHC: immunohistochemistry; TCGA: the Cancer Genome Atlas; RSEM: RNA-seq by Expectation Maximization; DAPI: 4′,6-diamidino-2-phenylindole; siNC: siRNA control; NT: nontreated cells; DOX: doxycycline; OE: overexpression; NC: negative control; CCK-8: Cell Counting Kit-8; SDS: sodium dodecyl sulfate; PI: propidium iodide; LC–MS/MS: liquid chromatography–mass spectrometry/mass spectrometry; m^{6}A-d3: *N*^{6}-methyladenosine-d3; A: adenosine; FDR: false discovery rate; GSEA: Gene set enrichment analysis; GEO: Gene Expression Omnibus; NCBI: National Center

for Biotechnology Information; SD: standard deviation; OS: Overall survival; RFS: recurrence-free survival; ANOVA: analysis of variance; DEGs: differentially expressed genes; LYPD1: LY6/PLAUR Domain Containing 1

References

1. WHO report on cancer: setting priorities, investing wisely and providing care for all [Available from: https://www.who.int/publications/i/item/who-report-on-cancer-setting-priorities-investing-wisely-and-providing-care-for-all.

2. Mok TS, Wu YL, Thongprasert S, Yang CH, Chu DT, Saijo N, et al. Gefitinib or carboplatin-paclitaxel in pulmonary adenocarcinoma. N Engl J Med. 2009;361(10):947-57.

3. Shaw AT, Kim DW, Nakagawa K, Seto T, Crino L, Ahn MJ, et al. Crizotinib versus chemotherapy in advanced ALK-positive lung cancer. N Engl J Med. 2013;368(25):2385-94.

4. Planchard D, Besse B, Groen HJM, Souquet P-J, Quoix E, Baik CS, et al. Dabrafenib plus trametinib in patients with previously treated BRAFV600E-mutant

826 metastatic non-small cell lung cancer: an open-label, multicentre phase 2 trial. The
827 Lancet Oncology. 2016;17(7):984-93.
828 5. Shaw AT, Ou SH, Bang YJ, Camidge DR, Solomon BJ, Salgia R, et al.
829 Crizotinib in ROS1-rearranged non-small-cell lung cancer. N Engl J Med.
830 2014;371(21):1963-71.
831 6. Gandhi L, Rodriguez-Abreu D, Gadgeel S, Esteban E, Felip E, De Angelis F, et
832 al. Pembrolizumab plus Chemotherapy in Metastatic Non-Small-Cell Lung Cancer. N
833 Engl J Med. 2018;378(22):2078-92.
834 7. Carroll SM, Narayan P, Rottman FM. N6-methyladenosine residues in an
835 intron-specific region of prolactin pre-mRNA. Mol Cell Biol. 1990;10(9):4456-65.
836 8. Dominissini D, Moshitch-Moshkovitz S, Schwartz S, Salmon-Divon M, Ungar
837 L, Osenberg S, et al. Topology of the human and mouse m6A RNA methylomes
838 revealed by m6A-seq. Nature. 2012;485(7397):201-6.
839 9. Liu J, Yue Y, Han D, Wang X, Fu Y, Zhang L, et al. A METTL3-METTL14
840 complex mediates mammalian nuclear RNA N6-adenosine methylation. Nat Chem Biol.
841 2014;10(2):93-5.

842 10. Ping XL, Sun BF, Wang L, Xiao W, Yang X, Wang WJ, et al. Mammalian
843 WTAP is a regulatory subunit of the RNA N6-methyladenosine methyltransferase. Cell
844 Research. 2014;24(2):177-89.
845 11. Yue Y, Liu J, Cui X, Cao J, Luo G, Zhang Z, et al. VIRMA mediates
846 preferential m(6)A mRNA methylation in 3'UTR and near stop codon and associates
847 with alternative polyadenylation. Cell Discov. 2018;4:10.
848 12. Patil DP, Chen CK, Pickering BF, Chow A, Jackson C, Guttman M, et al.
849 m(6)A RNA methylation promotes XIST-mediated transcriptional repression. Nature.
850 2016;537(7620):369-73.
851 13. Jia G, Fu Y, Zhao X, Dai Q, Zheng G, Yang Y, et al. N6-methyladenosine in
852 nuclear RNA is a major substrate of the obesity-associated FTO. Nat Chem Biol.
853 2011;7(12):885-7.
854 14. Zheng G, Dahl JA, Niu Y, Fedorcsak P, Huang CM, Li CJ, et al. ALKBH5 is a
855 mammalian RNA demethylase that impacts RNA metabolism and mouse fertility. Mol
856 Cell. 2013;49(1):18-29.
857 15. Mauer J, Luo X, Blanjoie A, Jiao X, Grozhik AV, Patil DP, et al. Reversible
858 methylation of m(6)Am in the 5' cap controls mRNA stability. Nature.
859 2017;541(7637):371-5.

16. Meyer KD, Saletore Y, Zumbo P, Elemento O, Mason CE, Jaffrey SR. Comprehensive analysis of mRNA methylation reveals enrichment in 3' UTRs and near stop codons. Cell. 2012;149(7):1635-46.

17. Tang C, Klukovich R, Peng H, Wang Z, Yu T, Zhang Y, et al. ALKBH5-dependent m6A demethylation controls splicing and stability of long 3'-UTR mRNAs in male germ cells. Proc Natl Acad Sci U S A. 2018;115(2):E325-E33.

18. Xiao W, Adhikari S, Dahal U, Chen YS, Hao YJ, Sun BF, et al. Nuclear m(6)A Reader YTHDC1 Regulates mRNA Splicing. Mol Cell. 2016;61(4):507-19.

19. Liu N, Dai Q, Zheng G, He C, Parisien M, Pan T. N(6)-methyladenosine-dependent RNA structural switches regulate RNA-protein interactions. Nature. 2015;518(7540):560-4.

20. Liu N, Zhou KI, Parisien M, Dai Q, Diatchenko L, Pan T. N6-methyladenosine alters RNA structure to regulate binding of a low-complexity protein. Nucleic Acids Res. 2017;45(10):6051-63.

21. Li A, Chen YS, Ping XL, Yang X, Xiao W, Yang Y, et al. Cytoplasmic m(6)A reader YTHDF3 promotes mRNA translation. Cell Res. 2017;27(3):444-7.

876 22. Choe J, Lin S, Zhang W, Liu Q, Wang L, Ramirez-Moya J, et al. mRNA
877 circularization by METTL3-eIF3h enhances translation and promotes oncogenesis.
878 Nature. 2018;561(7724):556-60.
879 23. Wang X, Zhao BS, Roundtree IA, Lu Z, Han D, Ma H, et al.
880 N(6)-methyladenosine Modulates Messenger RNA Translation Efficiency. Cell.
881 2015;161(6):1388-99.
882 24. Shi H, Wang X, Lu Z, Zhao BS, Ma H, Hsu PJ, et al. YTHDF3 facilitates
883 translation and decay of N(6)-methyladenosine-modified RNA. Cell Res.
884 2017;27(3):315-28.
885 25. Wang X, Lu Z, Gomez A, Hon GC, Yue Y, Han D, et al.
886 N6-methyladenosine-dependent regulation of messenger RNA stability. Nature.
887 2014;505(7481):117-20.
888 26. Huang H, Weng H, Sun W, Qin X, Shi H, Wu H, et al. Recognition of RNA
889 N(6)-methyladenosine by IGF2BP proteins enhances mRNA stability and translation.
890 Nat Cell Biol. 2018;20(3):285-95.
891 27. Ma L, Chen T, Zhang X, Miao Y, Tian X, Yu K, et al. The m(6)A reader
892 YTHDC2 inhibits lung adenocarcinoma tumorigenesis by suppressing
893 SLC7A11-dependent antioxidant function. Redox Biol. 2021;38:101801.

894 28. Zhang S, Zhao BS, Zhou A, Lin K, Zheng S, Lu Z, et al. m(6)A Demethylase
895 ALKBH5 Maintains Tumorigenicity of Glioblastoma Stem-like Cells by Sustaining
896 FOXM1 Expression and Cell Proliferation Program. Cancer Cell. 2017;31(4):591-606
897 e6.
898 29. Chen S, Zhou L, Wang Y. ALKBH5-mediated m(6)A demethylation of lncRNA
899 PVT1 plays an oncogenic role in osteosarcoma. Cancer Cell Int. 2020;20:34.
900 30. Guo T, Liu DF, Peng SH, Xu AM. ALKBH5 promotes colon cancer
901 progression by decreasing methylation of the lncRNA NEAT1. Am J Transl Res.
902 2020;12(8):4542-9.
903 31. Jiang Y, Wan Y, Gong M, Zhou S, Qiu J, Cheng W. RNA demethylase
904 ALKBH5 promotes ovarian carcinogenesis in a simulated tumour microenvironment
905 through stimulating NF-kappaB pathway. J Cell Mol Med. 2020;24(11):6137-48.
906 32. Nagaki Y, Motoyama S, Yamaguchi T, Hoshizaki M, Sato Y, Sato T, et al. m(6)
907 A demethylase ALKBH5 promotes proliferation of esophageal squamous cell carcinoma
908 associated with poor prognosis. Genes Cells. 2020;25(8):547-61.
909 33. Pu X, Gu Z, Gu Z. ALKBH5 regulates IGF1R expression to promote the
910 Proliferation and Tumorigenicity of Endometrial Cancer. J Cancer.
911 2020;11(19):5612-22.

912 34. Zhang X, Wang F, Wang Z, Yang X, Yu H, Si S, et al. ALKBH5 promotes the
913 proliferation of renal cell carcinoma by regulating AURKB expression in an
914 m(6)A-dependent manner. Ann Transl Med. 2020;8(10):646.
915 35. Chen Y, Zhao Y, Chen J, Peng C, Zhang Y, Tong R, et al. ALKBH5 suppresses
916 malignancy of hepatocellular carcinoma via m(6)A-guided epigenetic inhibition of
917 LYPD1. Mol Cancer. 2020;19(1):123.
918 36. Guo X, Li K, Jiang W, Hu Y, Xiao W, Huang Y, et al. RNA demethylase
919 ALKBH5 prevents pancreatic cancer progression by posttranscriptional activation of
920 PER1 in an m6A-YTHDF2-dependent manner. Mol Cancer. 2020;19(1):91.
921 37. Liu J, Ren D, Du Z, Wang H, Zhang H, Jin Y. m(6)A demethylase FTO
922 facilitates tumor progression in lung squamous cell carcinoma by regulating MZF1
923 expression. Biochem Biophys Res Commun. 2018;502(4):456-64.
924 38. Li J, Han Y, Zhang H, Qian Z, Jia W, Gao Y, et al. The m6A demethylase FTO
925 promotes the growth of lung cancer cells by regulating the m6A level of USP7 mRNA.
926 Biochem Biophys Res Commun. 2019;512(3):479-85.
927 39. Ding Y, Qi N, Wang K, Huang Y, Liao J, Wang H, et al. FTO Facilitates Lung
928 Adenocarcinoma Cell Progression by Activating Cell Migration Through mRNA
929 Demethylation. Onco Targets Ther. 2020;13:1461-70.

930 40. Jin D, Guo J, Wu Y, Yang L, Wang X, Du J, et al. m(6)A demethylase ALKBH5
931 inhibits tumor growth and metastasis by reducing YTHDFs-mediated YAP expression
932 and inhibiting miR-107/LATS2-mediated YAP activity in NSCLC. Mol Cancer.
933 2020;19(1):40.
934 41. Zhu Z, Qian Q, Zhao X, Ma L, Chen P. N(6)-methyladenosine ALKBH5
935 promotes non-small cell lung cancer progress by regulating TIMP3 stability. Gene.
936 2020;731:144348.
937 42. Zhang D, Ning J, Okon I, Zheng X, Satyanarayana G, Song P, et al.
938 Suppression of m6A mRNA modification by DNA hypermethylated ALKBH5
939 aggravates the oncological behavior of KRAS mutation/LKB1 loss lung cancer. Cell
940 Death Dis. 2021;12(6):518.
941 43. Zhang C, Samanta D, Lu H, Bullen JW, Zhang H, Chen I, et al. Hypoxia
942 induces the breast cancer stem cell phenotype by HIF-dependent and
943 ALKBH5-mediated m(6)A-demethylation of NANOG mRNA. Proc Natl Acad Sci U S
944 A. 2016;113(14):E2047-56.
945 44. Chao Y, Shang J, Ji W. ALKBH5-m(6)A-FOXM1 signaling axis promotes
946 proliferation and invasion of lung adenocarcinoma cells under intermittent hypoxia.
947 Biochem Biophys Res Commun. 2020;521(2):499-506.

948 45. Inoue Y, Matsuura S, Kurabe N, Kahyo T, Mori H, Kawase A, et al.
949 Clinicopathological and Survival Analysis of Japanese Patients with Resected
950 Non-Small-Cell Lung Cancer Harboring NKX2-1, SETDB1, MET, HER2, SOX2,
951 FGFR1, or PIK3CA Gene Amplification. Journal of Thoracic Oncology.
952 2015;10(11):1590-600.
953 46. Du C, Kurabe N, Matsushima Y, Suzuki M, Kahyo T, Ohnishi I, et al. Robust
954 quantitative assessments of cytosine modifications and changes in the expressions of
955 related enzymes in gastric cancer. Gastric Cancer. 2015;18(3):516-25.
956 47. Zhou Y, Zeng P, Li YH, Zhang Z, Cui Q. SRAMP: prediction of mammalian
957 N6-methyladenosine (m6A) sites based on sequence-derived features. Nucleic Acids
958 Res. 2016;44(10):e91.
959 48. Zhou Z, Lv J, Yu H, Han J, Yang X, Feng D, et al. Mechanism of RNA
960 modification N6-methyladenosine in human cancer. Mol Cancer. 2020;19(1):104.
961 49. National Center for Biotechnology Information, Gene, E2F1.
962 https://www.ncbi.nlm.nih.gov/gene/1869.
963 50. National Center for Biotechnology Information, Gene, CDKN1A.
964 https://www.ncbi.nlm.nih.gov/gene/1026.

965 51. National Center for Biotechnology Information, Gene, CCNG2.
966 https://www.ncbi.nlm.nih.gov/gene/901.
967 52. National Center for Biotechnology Information, Gene, CASP14.
968 https://www.ncbi.nlm.nih.gov/gene/23581.
969 53. National Center for Biotechnology Information, Gene, PMAIP1.
970 https://www.ncbi.nlm.nih.gov/gene/5366.
971 54. National Center for Biotechnology Information, Gene, AKAP12.
972 https://www.ncbi.nlm.nih.gov/gene/9590.
973 55. Carrier F, Smith ML, Bae I, Kilpatrick KE, Lansing TJ, Chen CY, et al.
974 Characterization of human Gadd45, a p53-regulated protein. J Biol Chem.
975 1994;269(51):32672-7.
976 56. Xue X, Fei X, Hou W, Zhang Y, Liu L, Hu R. miR-342-3p suppresses cell
977 proliferation and migration by targeting AGR2 in non-small cell lung cancer. Cancer
978 Lett. 2018;412:170-8.
979 57. Gan R, Yang Y, Yang X, Zhao L, Lu J, Meng QH. Downregulation of
980 miR-221/222 enhances sensitivity of breast cancer cells to tamoxifen through
981 upregulation of TIMP3. Cancer Gene Ther. 2014;21(7):290-6.

982 58. Wang JL, Chen ZF, Chen HM, Wang MY, Kong X, Wang YC, et al. Elf3 drives
983 beta-catenin transactivation and associates with poor prognosis in colorectal cancer. Cell
984 Death Dis. 2014;5:e1263.
985 59. Tsuchiya K, Yoshimura K, Inoue Y, Iwashita Y, Yamada H, Kawase A, et al.
986 YTHDF1 and YTHDF2 are associated with better patient survival and an inflamed
987 tumor-immune microenvironment in non-small-cell lung cancer. Oncoimmunology.
988 2021;10(1):1962656.
989 60. Abbas T, Dutta A. p21 in cancer: intricate networks and multiple activities. Nat
990 Rev Cancer. 2009;9(6):400-14.
991 61. Su CW, Lin CW, Yang WE, Yang SF. TIMP-3 as a therapeutic target for cancer.
992 Ther Adv Med Oncol. 2019;11:1758835919864247.
993 62. Lei Y, Liu Z, Yang W. Negative correlation of cytoplasm TIMP3 with miR-222
994 indicates a good prognosis for NSCLC. Onco Targets Ther. 2018;11:5551-7.
995 63. Garofalo M, Di Leva G, Romano G, Nuovo G, Suh SS, Ngankeu A, et al.
996 miR-221&222 regulate TRAIL resistance and enhance tumorigenicity through PTEN
997 and TIMP3 downregulation. Cancer Cell. 2009;16(6):498-509.
998 64. Huang X, Zhang H, Guo X, Zhu Z, Cai H, Kong X. Insulin-like growth factor
999 2 mRNA-binding protein 1 (IGF2BP1) in cancer. J Hematol Oncol. 2018;11(1):88.

65. Kato T, Hayama S, Yamabuki T, Ishikawa N, Miyamoto M, Ito T, et al. Increased expression of insulin-like growth factor-II messenger RNA-binding protein 1 is associated with tumor progression in patients with lung cancer. Clin Cancer Res. 2007;13(2 Pt 1):434-42.

66. Huang RS, Zheng YL, Li C, Ding C, Xu C, Zhao J. MicroRNA-485-5p suppresses growth and metastasis in non-small cell lung cancer cells by targeting IGF2BP2. Life Sci. 2018;199:104-11.

67. Findeis-Hosey JJ, Yang Q, Spaulding BO, Wang HL, Xu H. IMP3 expression is correlated with histologic grade of lung adenocarcinoma. Hum Pathol. 2010;41(4):477-84.

68. Findeis-Hosey JJ, Xu H. Insulin-like growth factor II-messenger RNA-binding protein-3 and lung cancer. Biotech Histochem. 2012;87(1):24-9.

69. Zhao W, Lu D, Liu L, Cai J, Zhou Y, Yang Y, et al. Insulin-like growth factor 2 mRNA binding protein 3 (IGF2BP3) promotes lung tumorigenesis via attenuating p53 stability. Oncotarget. 2017;8(55):93672-87.

70. Cui Q, Shi H, Ye P, Li L, Qu Q, Sun G, et al. m(6)A RNA Methylation Regulates the Self-Renewal and Tumorigenesis of Glioblastoma Stem Cells. Cell Rep. 2017;18(11):2622-34.

71. Huang Y, Su R, Sheng Y, Dong L, Dong Z, Xu H, et al. Small-Molecule Targeting of Oncogenic FTO Demethylase in Acute Myeloid Leukemia. Cancer Cell. 2019;35(4):677-91 e10.

72. Li N, Kang Y, Wang L, Huff S, Tang R, Hui H, et al. ALKBH5 regulates anti-PD-1 therapy response by modulating lactate and suppressive immune cell accumulation in tumor microenvironment. Proc Natl Acad Sci U S A. 2020;117(33):20159-70.

Declarations

Acknowledgments

We are grateful to the patients and sample donors for their dedicated participation in this study. We also thank Takaharu Kamo, Shiho Omori, Hisaki Igarashi (Tumor Pathology, Hamamatsu University School of Medicine), Ryo Horiguchi, Masako Suzuki, and Takuya Kitamoto (Advanced Research Facilities and Services, Hamamatsu University School of Medicine) for providing technical assistance.

Author contributions

HS conceived this project, supervised all experiments and interpretations, and drafted the manuscript. KT designed and performed all experiments, analyzed the data, interpreted patient and experimental data, and drafted the manuscript. KY designed this project, performed sample collection, histological examination, and a part of the experiments, and drafted the manuscript. Yusuke Inoue performed sample collection and histological examination. Yuji Iwashita designed this project, interpreted the experimental data, and drafted the manuscript. TO performed molecular experiments, interpreted the experimental data, and drafted the manuscript. HY and HW assisted part of the experiments. AK, MT, HO, and KF performed sample collection. KS performed sample collection and analyzed data. TS supervised this project. All authors have read and approved the final manuscript.

Funding

This work was supported by grants from the Japan Society for the Promotion of Science (JP22659072, JP24659161, JP26670187, JP16K15256) and HUSM Grant-in-Aid, and Smoking Research Foundation.

Availability of data and materials

All data and supplementary information within the article are available from the published article (including supplementary information files) or available on published databases (TCGA or GEO). GEO accession numbers of our microarray data are GSE165453 and GSE165453.

Ethics approval and consent to participate

This study was approved by the Ethics Committees of Hamamatsu University School of Medicine (20-011) and Seirei Mikatahara General Hospital and was carried out in accordance with approved guidelines. Written informed consent was obtained from all patients. All analyses were conducted in compliance with the ethical standards according to the Helsinki Declaration.

Consent for publication

Not applicable.

Competing interests

The authors declare no competing interests.

Figure legends

Figure 1. High ALKBH5 expression was associated with a worse prognosis in patients with non-small-cell lung cancer.

(**A**) ALKBH5 and FTO mRNA levels were analyzed in the paired non-cancerous and NSCLC tissues using the TCGA database (n = 109 for each group). (**B**) ALKBH5 and FTO protein levels were assessed in the paired non-cancerous lung alveolar tissue and NSCLC tissues in the HUSM cohort via immunohistochemistry (IHC) using the H-score (n = 77 for each group). (**C**) Relative ALKBH5 and FTO mRNA expression levels were detected using qPCR in cell lines. Data were normalized to GAPDH and adjusted to the expression of BEAS2B cells (ALKBH5: n = 2, FTO: n = 3). (**D**) ALKBH5 and FTO protein expression levels were determined using western blot analysis in cell lines. (**E**) IHC staining for ALKBH5 and FTO were assessed using the TMA core of NSCLC tissues in the HUSM cohort. Staining intensity was categorized into 0 (absent), 1 (weak), 2 (moderate), or 3 (strong). (**F**) Immunofluorescence visualized subcellular localization in PC9 cells (×100). PC9 cells infected with pRetroX-TetOne puro- ALKBH5 were transduced by 100 ng/mL of doxycycline and

1089 used as ALKBH5 overexpression. PC9 cells without doxycycline were used as a
1090 negative control. (**G**) A Kaplan–Meier survival curve with a log-rank test was utilized to
1091 analyze the overall survival of the HUSM cohort. Patients were stratified into low (blue)
1092 or high-expression groups (red) based on a cutoff determined by the median H-scores (n
1093 = 627). Results were presented as the median (A and B) or mean ± SD (c). ****$P <$
1094 0.0001 indicates a significant difference between the indicated groups.
1095
1096 **Figure 2. ALKBH5 knockdown suppressed cell proliferation in non-small-cell lung**
1097 **cancer**
1098 (**A, B**) Western blot analysis demonstrated ALKBH5 protein levels in cells transfected
1099 with siRNA for ALKBH5 (siALKBH5), FTO (siFTO), control (siNC), or nontreated
1100 cells (NT). (**C**) Cell proliferation relative to baseline in PC9 and A549 cells transfected
1101 with siALKBH5 (#1 and #3) or siNC were assessed using the CCK-8 assay (n = 3). **(D)**
1102 Cell proliferation relative to baseline in PC9 and A549 cells transfected with siFTO (#1
1103 and #3) or siNC were assessed using the CCK-8 assay (n = 3). (**E**) The migration ability
1104 of PC9 and A549 cells transfected with siALKBH5 (#1 and #3) or siNC were assessed
1105 using transwell migration assay. The bar charts indicate the number of migratory cells
1106 that passed through the chamber membrane (n = 3). (**F, G**) The migration ability of PC9

(**F**) and A549 (**G**) cells transfected with siALKBH5 (#1 and #3) or siNC was assessed using wound-healing assay (n = 3). Results were presented as mean ± SD. $^{**}P < 0.01$, $^{***}P < 0.001$, $^{****}P < 0.0001$ indicates a significant difference between the indicated groups.

Figure 3. ALKBH5 knockdown-induced G1 phase arrest of cell cycle and/or apoptosis in non-small-cell lung cancer

(**A–D**) The cell cycle was examined via flow cytometry with PC9 (A) and A549 (C) cells transfected with siALKBH5 (#1 and #3) or siNC. The bar charts indicate the percentage of cells in each cell cycle phase [n = 6 for PC9 (B), n = 3 for A549 cells (D)]. (**E** and **F**) Apoptotic cells were determined using flow cytometric analysis of PC9 cells transfected with siALKBH5 (#1 and #3) or siNC. (E) Percentage of the apoptotic cells in which both propidium iodide and annexin V were positive are shown in a representative scatter plot. (F) The apoptosis rate in ALKBH5 knockdown was compared with siNC and shown as a bar chart (n = 3). (**G** and **H**) Cisplatin- or gefitinib-induced apoptotic cells were determined via flow cytometry with PC9 cells transfected with siALKBH5 or siNC. (G) Percentage of apoptotic cells shown in a representative scatter plot. (H) The cisplatin- or gefitinib-induced apoptosis rate in

ALKBH5 knockdown was compared with siNC and shown as a bar chart (n = 3). (**I** and **J**) Apoptotic cells were determined via flow cytometry with A549 cells transfected with siALKBH5 or siNC. (I) Percentage of the apoptotic cells shown in a representative scatter plot. (J) Apoptosis rate in ALKBH5 knockdown was compared with siNC and shown as a bar chart (n = 6). (**K** and **L**) Cisplatin-induced apoptotic cells were determined via flow cytometric analysis of A549 cells transfected with siALKBH5 or siNC. (K) Percentage of the apoptotic cells shown in a representative scatter plot. (L) The cisplatin-induced apoptosis rate in ALKBH5 knockdown was compared with siNC and shown as a bar chart (n = 3). Results were presented as mean ± SD. $^{*}P < 0.05$, $^{**}P < 0.01$, $^{***}P < 0.001$, $^{****}P < 0.0001$ indicates a significant difference between the indicated groups.

Figure 4. ALKBH5 overexpression promoted cell proliferation

Immortalized cells infected with pRetroX-TetOne puro empty vector (empty) or pRetroX-TetOne puro-ALKBH5 (ALKBH5) were used to assess the function of ALKBH5-overexpressed cells. The concentration of doxycycline (DOX) was 100 ng/mL. (**A**) Western blot analysis demonstrated ALKBH5 protein levels in ALKBH5-overexpressed HEK293 and BEAS2B cells. (**B, C**) Cells infected with

pRetroX-TetOne puro-ALKBH5 with DOX were designated as ALKBH5 overexpression (OE), whereas those without DOX were designated as negative control (NC). Cell proliferation relative to baseline in ALKBH5 OE HEK293 and BEAS2B cells were assessed using the CCK-8 assay (n = 3). (**D–G**) The migration ability of HEK293 and BEAS2B cells was assessed via wound-healing assay. Representative images of the wound-healing assay for HEK293 (**D**) and BEAS2B (**F**) cells. Wound areas relative to baseline at each time point were compared between ALKBH5 OE and NC HEK293 (**E**) and BEAS2B (**G**) cells (n = 3). Results are presented as mean ± SD. **P* < 0.05 indicates a significant difference between the indicated groups.

Figure 5. ALKBH5 altered the abundance of m^{6}A modification in polyA-enriched RNA

(**A**) Representative chromatograms obtained using liquid chromatography–mass spectrometry/mass spectrometry (LC–MS/MS) for adenosine (upper panel, 2.89 min), N^6-methyladenosine (middle panel, 3.81 min), and N^6-methyladenosine-d3 (lower panel, 3.76 min) in polyA-enriched RNA extracted from PC9 cells. Peak areas were quantified as the product of retention time (min) and count per seconds (cps). (**B** and **C**) The peak areas of m^{6}A were normalized to that of m6A-d3. The amount of m^{6}A in PC9 (B) and

A549 (C) cells transfected with siALKBH5 was compared with that in cells transfected with siNC for 48, 72, and 96 h (n = 3). (**D**) PolyA-enriched RNAs were extracted from PC9 cells containing pRetroX-TetOne puro-ALKBH5 vector. m^6A/m^6A-d3 in the cells incubated with various concentrations of DOX for 48 h were compared with that in cells incubated with 0 ng/mL DOX (n = 3). (**E**) m^6A/m^6A-d3 in PC9 cells containing pRetroX-TetOne puro-ALKBH5 vector (ALKBH5 OE) whose ALKBH5 overexpression was induced by 100 ng/mL DOX for 24, 48, 72, 96, 120 h was compared with those without DOX (NC) (n = 3). (**F**) m^6A/m^6A-d3 in HEK293 and BEAS2B (ALKBH5 OE) cells whose ALKBH5 overexpression was induced by 100 ng/mL DOX for 48 h were compared with those without DOX (NC) (n = 3). Results were presented as mean ± SD. **P* < 0.05, ***P* < 0.01, ****P* < 0.001, *****P* < 0.0001 indicates a significant difference between the indicated groups by Student's *t*-test.

Figure 6. ALKBH5 knockdown regulated cell proliferation-related genes and m^6A abundance in the 3′ untranslated regions of specific genes

PC9 cells were transfected with siNC, siALKBH5#1, or siALKBH5#3 for 96 h (n = 3 for each group). (**A, B**) Differentially expressed genes (DEGs) for siALKBH5#1 (A) or siALKBH5#3 (B) were detected using expression microarray and shown using volcano

plots. Dashed lines indicate the threshold for the differential expression [fold change > 1.5 (log2 fold change = 0.5849) or < 0.67 (log2 fold change = −0.5849), $P < 0.01$ via Student's *t*-test] for upregulated (pink dots) or downregulated (light blue dots) genes. (**C**) Venn diagram indicating the number of common DEGs in ALKBH5-knockdown cells with different siRNA sequences. (**D**) mRNA expression levels of genes related to cell proliferation in ALKBH5-knockdown PC9 cells were analyzed using qPCR. Gene expression was normalized to the GAPDH expression and was shown relative to the expression with siNC. (**E**) m^6A level in the 3′ UTRs of target mRNA in PC9 cells transfected with siALKBH5#1 or siALKBH5#3 was quantified via MeRIP qPCR using anti-m6A antibody and was compared with that in cell transfected with siNC. The m^6A level was normalized to that of the input fraction (n = 3). IgG was used to evaluate the nonspecific binding of the target mRNA. (F; Upper panel) Prediction scores of m^6A modification in the CDKN1A and TIMP3 genes were calculated using the SRAMP algorithm. The combined scores were distributed through the full-length mRNA as different levels of very high, high, moderate, and low confidence. Arrows show the location of qPCR primers. Adenosines in consensus sequences for m^6A modification are presented in red. (Lower panel) PolyA-enriched RNA extracted from PC9 cells transfected with siALKBH5#1, siALKBH5#3, or siNC (n = 3) was immunoprecipitated

using anti-m^{6}A antibody or normal IgG. The m^{6}A level was calculated from transcript abundance in input or MeRIP fraction quantified using qPCR. Results are presented as mean ± SD. *P < 0.05, **P < 0.01, ***P < 0.001, ****P < 0.0001 indicates a significant difference between the indicated groups.

Figure 7. CDKN1A and TIMP3 were targets of m^{6}A modification via ALKBH5

(A) A schematic outline showing the workflow for the analysis of downstream targets of ALKBH5. (**B**) Target protein levels in PC9 or A549 cells transfected with siALKBH5#1 or siALKBH5#3 were compared with those transfected with siNC via western blot analysis. (**C**) Western blot analysis demonstrated CDKN1A (p21) or TIMP3 protein levels in PC9 cells transfected with siALKBH5, siCDKN1A, both siALKBH5 and siCDKN1A, or siNC. (**D**) Western blot analysis demonstrated TIMP3 protein levels in A549 cells transfected with siALKBH5, siTIMP3, both siALKBH5 and siTIMP3, or siNC. (**E** and **F**) Cell proliferation relative to baseline in PC9 (E) and A549 (F) cells transfected with siALKBH5 was assessed via the CCK-8 assay and compared with that in cells cotransfected with siALKBH5 and siCDKN1A or siTIMP3 (n = 3). ***P < 0.001, ****P < 0.0001 indicates a significant difference between the indicated groups.

Figure 8. IGF2BPs was required for the ALKBH5-induced regulation of mRNA expression and cell proliferation

(**A**) Expression levels of IGF2BP1, IGF2BP2, and IGF2BP3 (IGF2BPs) protein determined using western blot analysis were compared between cell lines. (**B**) IGF2BP protein levels in cells transfected with siALKBH5 (left end), those in cells transfected with siIGF2BP1, siIGF2BP2, or siIGF2BP3 with or without siALKBH5 (middle two lanes), or those with siNC (right end indicating both siALKBH5 and siIGF2BPs were negative) were confirmed via western blot analysis. (**C**) Relative mRNA expression levels of CDKN1A in PC9 cells or those of TIMP3 in A549 cells transfected with siALKBH5 were analyzed via qPCR and compared with those in cells cotransfected with siALKBH5 and one of the siIGF2BPs. Gene expression was normalized to the GAPDH expression and was shown relative to the expression in siNC (n = 3). (**D**) Expression levels of YTHDF2 protein determined using western blot analysis were compared between cell lines. (**E**) Relative mRNA expression levels of CDKN1A in PC9 cells or those of TIMP3 in A549 cells transfected with siALKBH5 were analyzed via qPCR and compared with those in cells cotransfected with siALKBH5 and siYTHDF2. Gene expression was normalized to the GAPDH expression and was shown relative to

the expression in siNC (n = 3). (**F**) The remaining RNA level of CDKN1A in PC9 cells or of TIMP3 in A549 cells after actinomycin D treatment for 0, 2, 4, and 6 h was determined using qPCR and normalized to the expression at 0 h. RNA decay rate in cells transfected with siALKBH5 and/or one of the siIGF2BPs and siNC were compared with the stability of CDKN1A and TIMPs (n = 3). (**G**) Cell proliferation relative to baseline in PC9 and A549cells transfected with siALKBH5 was assessed via the CCK-8 assay and compared with that in cells cotransfected with siALKBH5 and one of the siIGF2BPs (n = 3). (**H**) Schematic illustration for the proposed mechanism of tumorigenicity via ALKBH5 in non-small-cell lung cancer. Upregulation of ALKBH5 in NSCLC reduces m^6A modifications on the 3′ UTR of specific genes. The loss of m^6A decreases the opportunity for recognition by IGF2BPs and destabilizes the target transcripts such as CDKN1A (p21) and TIMP3. Downregulation of CDKN1A (p21) and TIMP3 induces cell cycle alteration and inhibits apoptosis. This ALKBH5–IGF2BPs axis promotes cell proliferation and tumorigenicity, which, in turn, causes the unfavorable prognosis of NSCLC. Results are presented as mean ± SD. $^{*}P < 0.05$, $^{**}P < 0.01$, $^{***}P < 0.001$, $^{****}P < 0.0001$ indicates a significant difference between the indicated groups.

1251

Figure 1

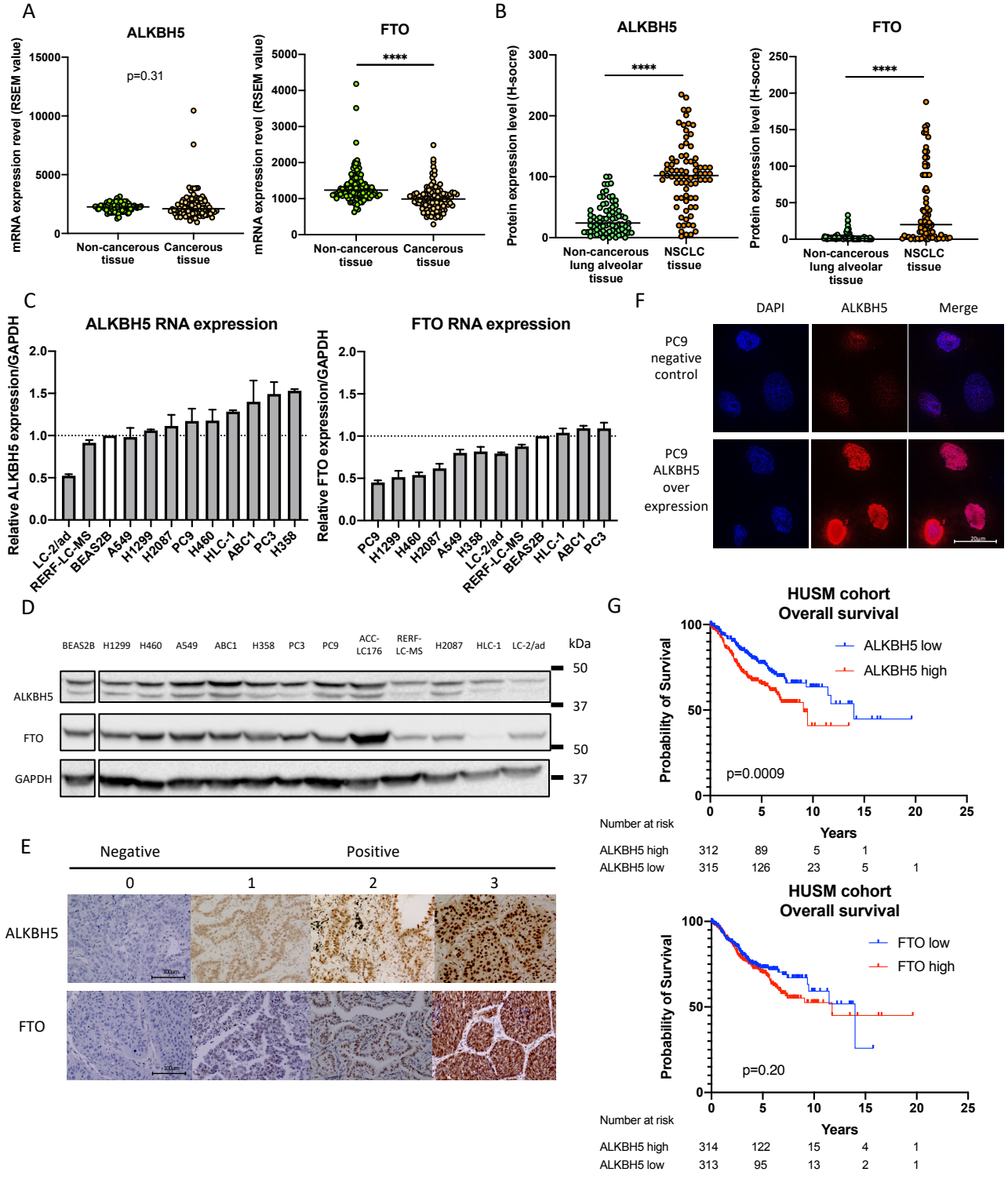
A
ALKBH5
p=0.31
mRNA expression revel (RSEM value)
Non-cancerous tissue
Cancerous tissue
FTO
****
B
ALKBH5
FTO
Protein expression level (H-socre)
Non-cancerous lung alveolar tissue
NSCLC tissue
C
ALKBH5 RNA expression
FTO RNA expression
Relative ALKBH5 expression/GAPDH
Relative FTO expression/GAPDH
LC-2/ad
RERF-LC-MS
BEAS2B
A549
H1299
H2087
PC9
H460
HLC-1
ABC1
PC3
H358
D
BEAS2B H1299 H460 A549 ABC1 H358 PC3 PC9 ACC-LC176 RERF-LC-MS H2087 HLC-1 LC-2/ad
kDa
ALKBH5
FTO
GAPDH
50
37
E
Negative
Positive
0
1
2
3
F
DAPI
ALKBH5
Merge
PC9 negative control
PC9 ALKBH5 over expression
G
HUSM cohort
Overall survival
ALKBH5 low
ALKBH5 high
Probability of Survival
p=0.0009
Years
Number at risk
ALKBH5 high 312 89 5 1
ALKBH5 low 315 126 23 5 1
FTO low
FTO high
p=0.20
ALKBH5 high 314 122 15 4 1
ALKBH5 low 313 95 13 2 1

Figure 2

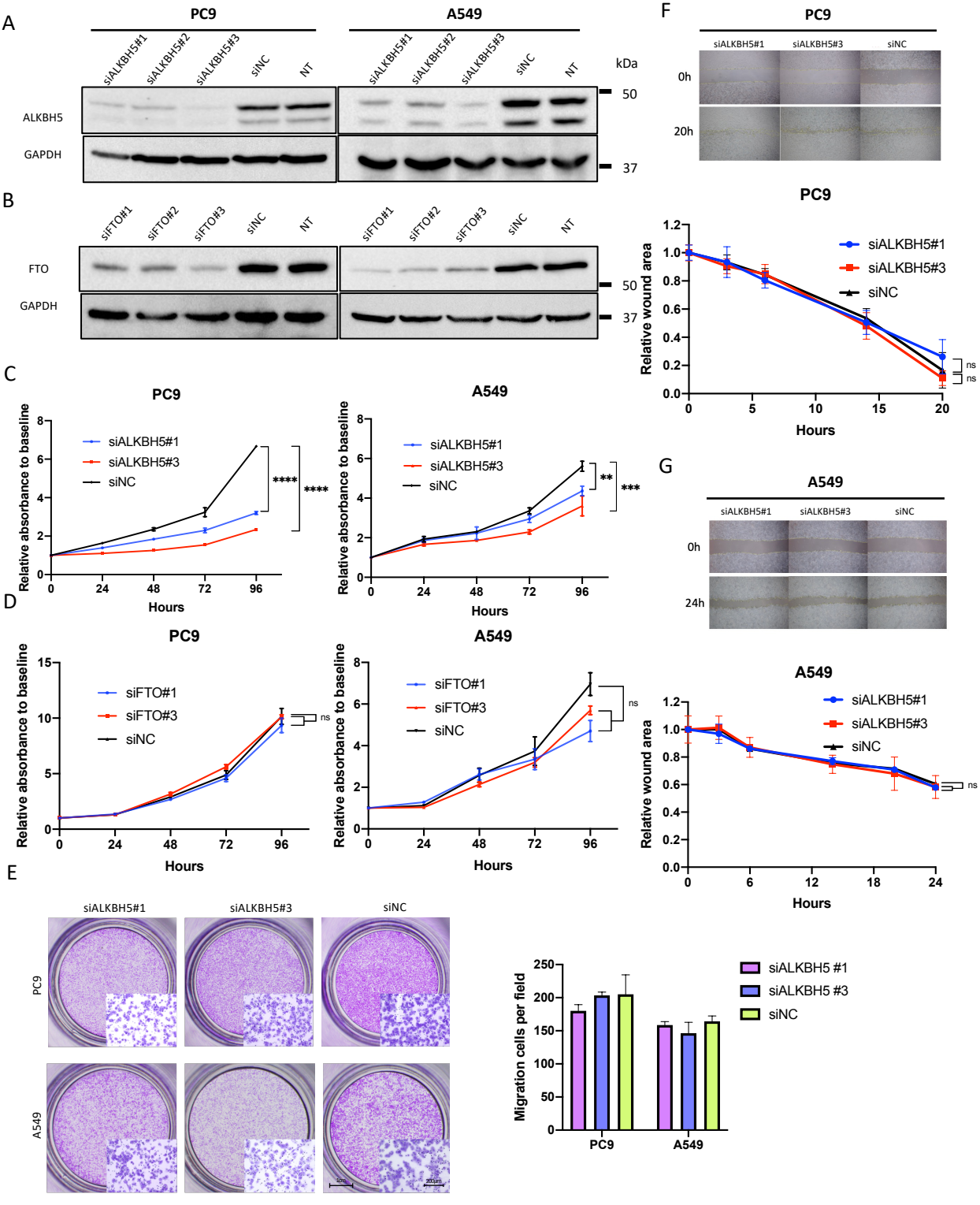
A
PC9
A549
siALKBH5#1
siALKBH5#2
siALKBH5#3
siNC
NT
kDa
ALKBH5
GAPDH
50
37
B
siFTO#1
siFTO#2
siFTO#3
FTO
C
Relative absorbance to baseline
Hours
siALKBH5#1
siALKBH5#3
siNC
****
**
***
D
siFTO#1
siFTO#3
ns
E
Migration cells per field
F
0h
20h
Relative wound area
G
24h

Figure 3

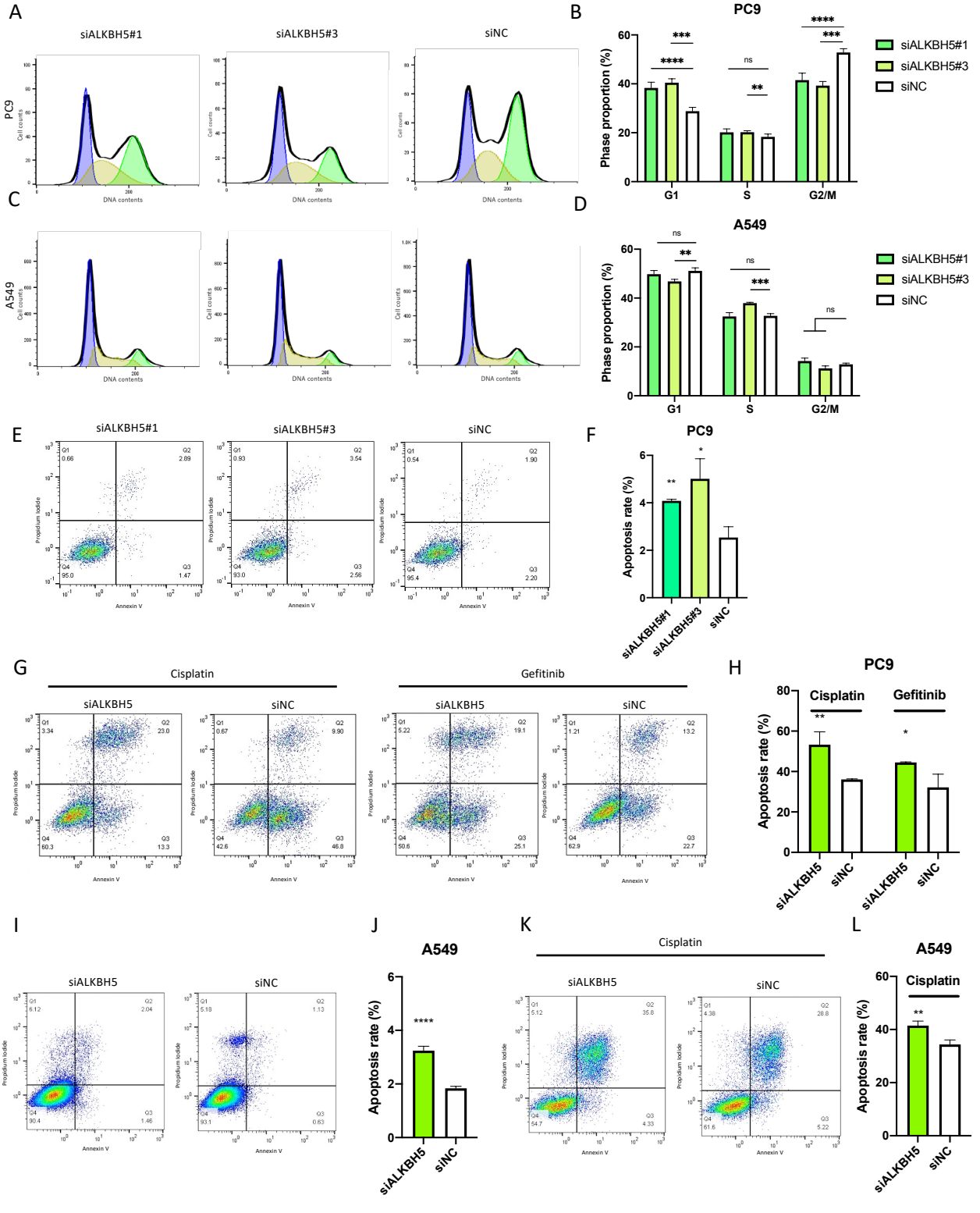
A
siALKBH5#1
siALKBH5#3
siNC
PC9
Cell counts
DNA contents
B
PC9
Phase proportion (%)
G1
S
G2/M
siALKBH5#1
siALKBH5#3
siNC
C
A549
D
A549
E
siALKBH5#1
siALKBH5#3
siNC
Propidium Iodide
Annexin V
F
PC9
Apoptosis rate (%)
G
Cisplatin
Gefitinib
siALKBH5
siNC
H
PC9
Cisplatin
Gefitinib
I
siALKBH5
siNC
J
A549
K
Cisplatin
siALKBH5
siNC
L
A549
Cisplatin

Figure 4

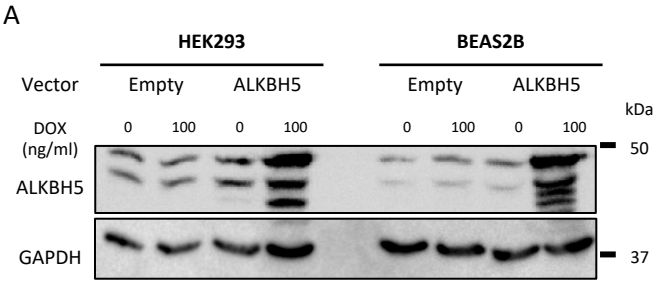
A
HEK293
BEAS2B
Vector
Empty
ALKBH5
Empty
ALKBH5
kDa
DOX (ng/ml)
0
100
0
100
0
100
0
100
ALKBH5
GAPDH
50
37

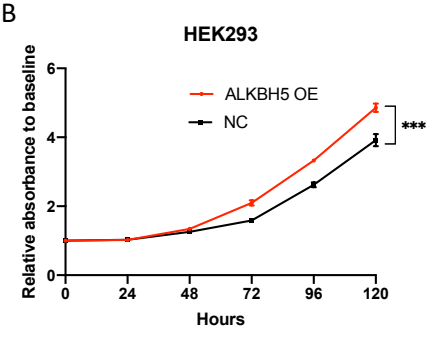
B
HEK293
ALKBH5 OE
NC
***
Relative absorbance to baseline
Hours
0
24
48
72
96
120

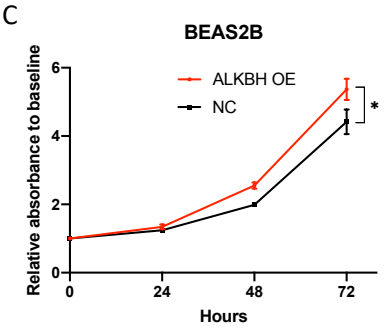
C
BEAS2B
ALKBH OE
NC
*
Relative absorbance to baseline
Hours
0
24
48
72

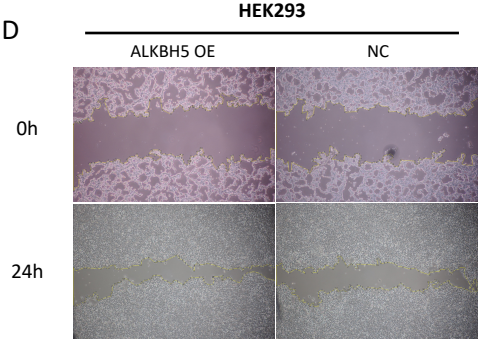
D
HEK293
ALKBH5 OE
NC
0h
24h

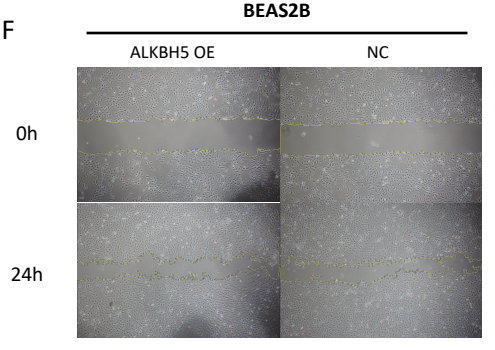
F
BEAS2B
ALKBH5 OE
NC
0h
24h

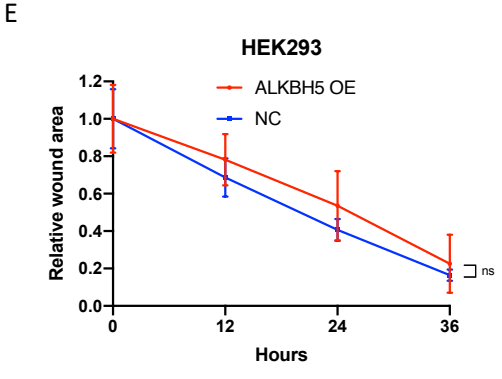
E
HEK293
ALKBH5 OE
NC
ns
Relative wound area
Hours
0
12
24
36

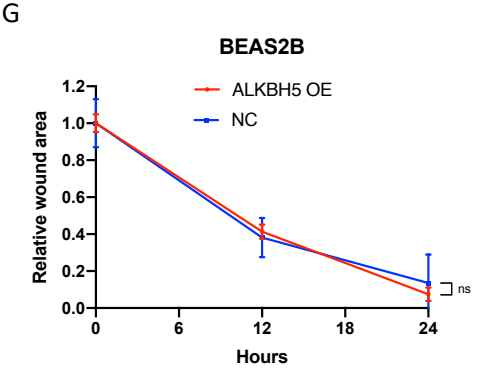
G
BEAS2B
ALKBH5 OE
NC
ns
Relative wound area
Hours
0
6
12
18
24

Figure 5

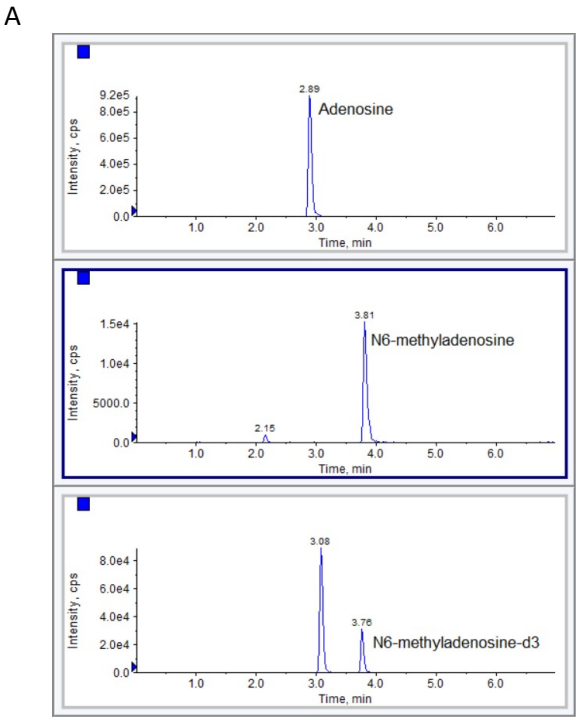
A
Adenosine
2.89
N6-methyladenosine
3.81
2.15
N6-methyladenosine-d3
3.08
3.76
Intensity, cps
Time, min

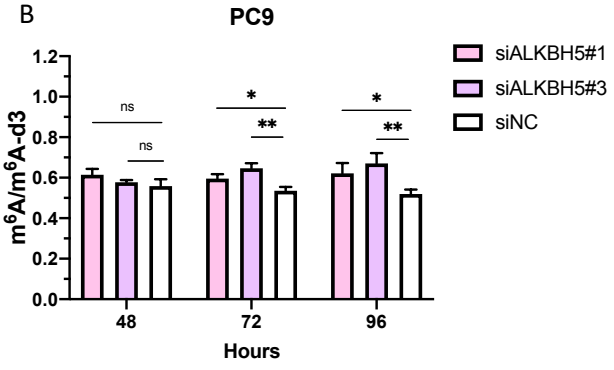
B
PC9
siALKBH5#1
siALKBH5#3
siNC
m6A/m6A-d3
Hours
ns
*
**

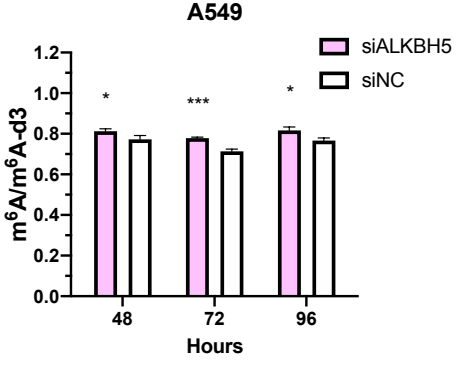
C
A549
siALKBH5
siNC
m6A/m6A-d3
Hours

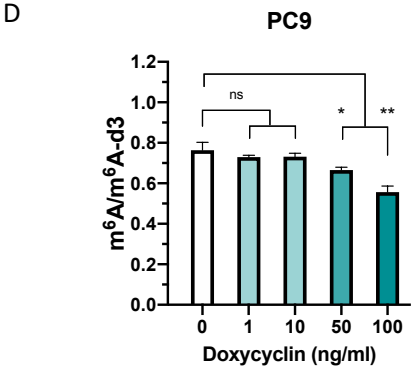
D
PC9
m6A/m6A-d3
Doxycyclin (ng/ml)
ns
*
**

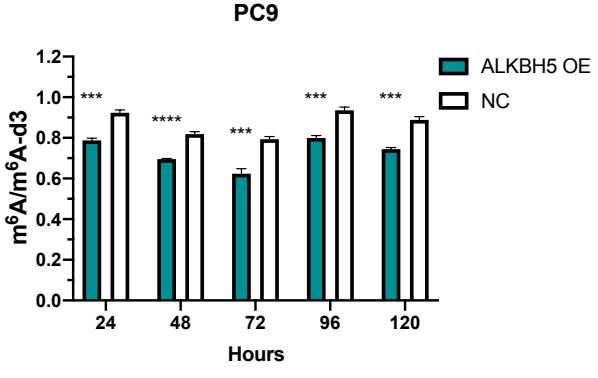
E
PC9
ALKBH5 OE
NC
m6A/m6A-d3
Hours

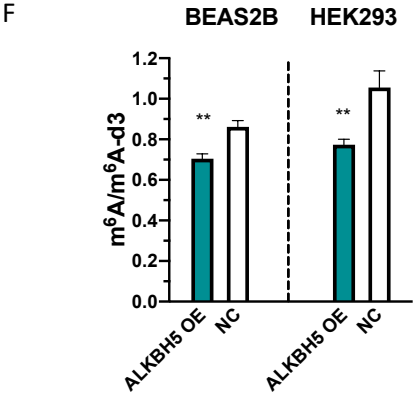
F
BEAS2B
HEK293
m6A/m6A-d3
ALKBH5 OE
NC

Figure 6

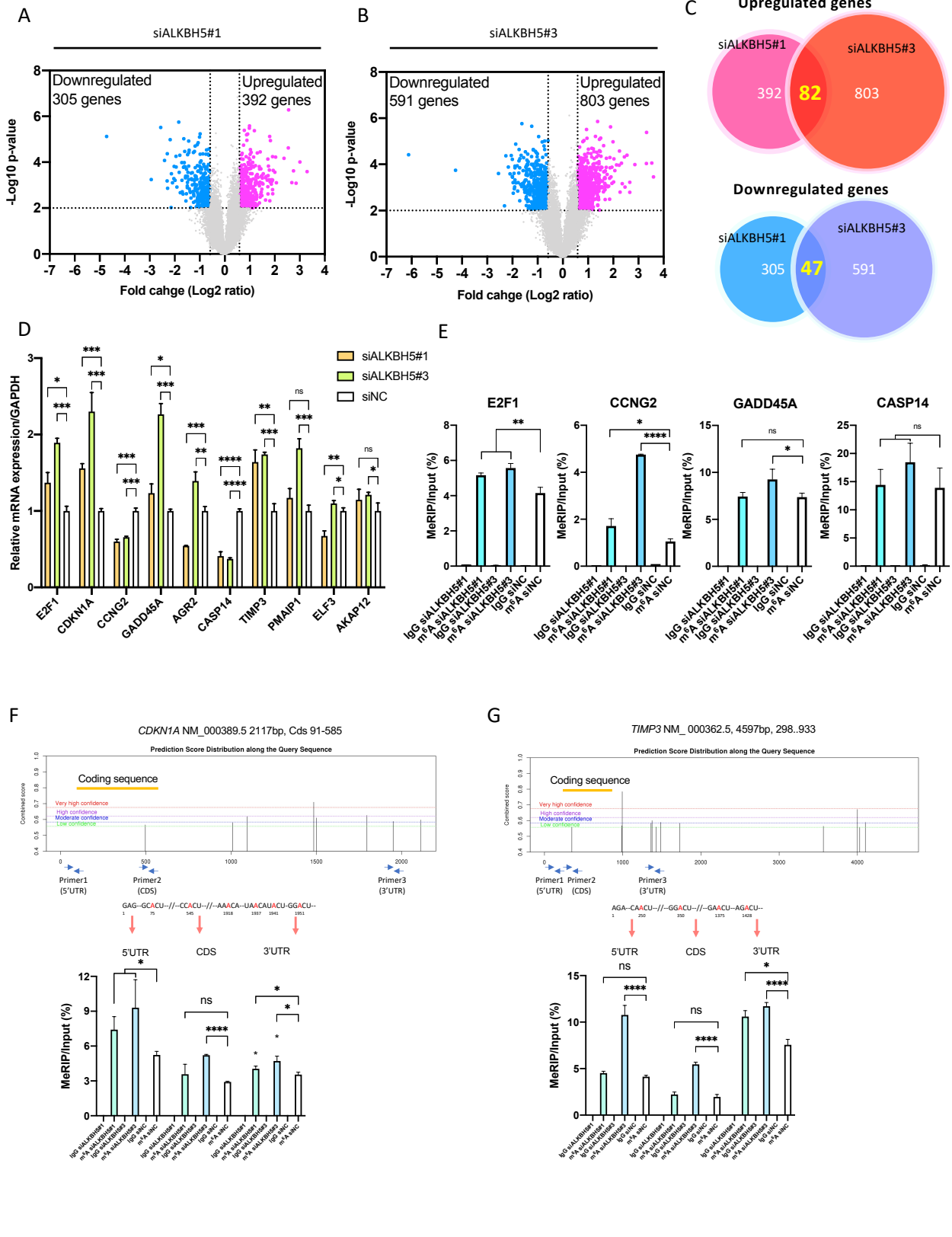
A
siALKBH5#1
Downregulated
305 genes
Upregulated
392 genes
-Log10 p-value
Fold cahge (Log2 ratio)
B
siALKBH5#3
Downregulated
591 genes
Upregulated
803 genes
-Log10 p-value
Fold cahge (Log2 ratio)
C
Upregulated genes
siALKBH5#1
siALKBH5#3
392
82
803
Downregulated genes
siALKBH5#1
siALKBH5#3
305
47
591
D
siALKBH5#1
siALKBH5#3
siNC
Relative mRNA expression/GAPDH
E2F1
CDKN1A
CCNG2
GADD45A
AGR2
CASP14
TIMP3
PMAIP1
ELF3
AKAP12
E
E2F1
CCNG2
GADD45A
CASP14
MeRIP/Input (%)
IgG siALKBH5#1
m⁶A siALKBH5#1
IgG siALKBH5#3
m⁶A siALKBH5#3
IgG siNC
m⁶A siNC
F
CDKN1A NM_000389.5 2117bp, Cds 91-585
Prediction Score Distribution along the Query Sequence
Coding sequence
Very high confidence
High confidence
Moderate confidence
Low confidence
Combined score
Primer1 (5'UTR)
Primer2 (CDS)
Primer3 (3'UTR)
5'UTR
CDS
3'UTR
MeRIP/Input (%)
G
TIMP3 NM_ 000362.5, 4597bp, 298..933
Prediction Score Distribution along the Query Sequence
Coding sequence
Very high confidence
High confidence
Moderate confidence
Low confidence
Combined score
Primer1 (5'UTR)
Primer2 (CDS)
Primer3 (3'UTR)
5'UTR
CDS
3'UTR
MeRIP/Input (%)

Figure 7

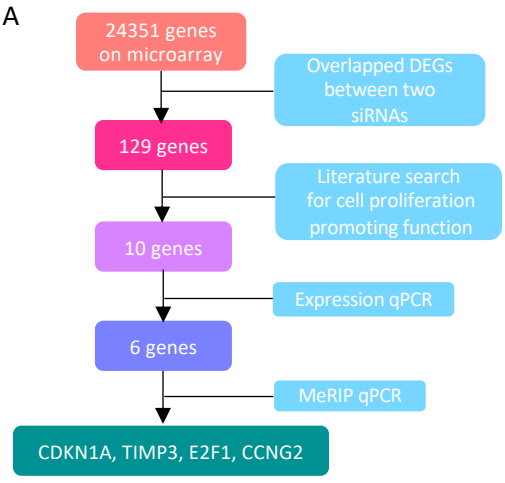
A
24351 genes on microarray
Overlapped DEGs between two siRNAs
129 genes
Literature search for cell proliferation promoting function
10 genes
Expression qPCR
6 genes
MeRIP qPCR
CDKN1A, TIMP3, E2F1, CCNG2

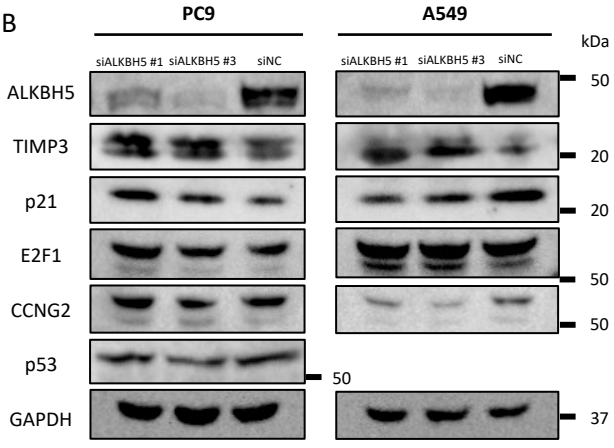
B
PC9
A549
kDa
siALKBH5 #1
siALKBH5 #3
siNC
ALKBH5
TIMP3
p21
E2F1
CCNG2
p53
GAPDH
50
20
20
50
50
50
37

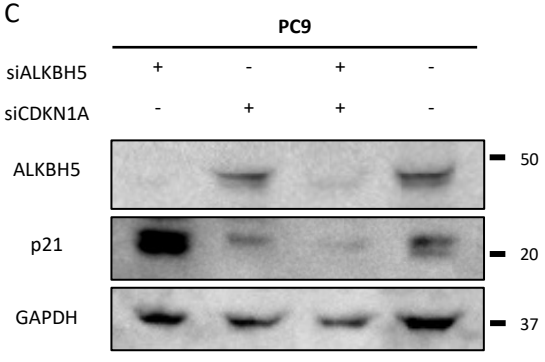
C
PC9
siALKBH5
siCDKN1A
ALKBH5
p21
GAPDH
50
20
37

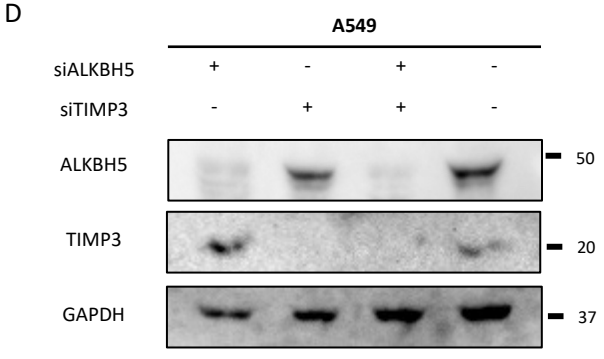
D
A549
siALKBH5
siTIMP3
ALKBH5
TIMP3
GAPDH
50
20
37

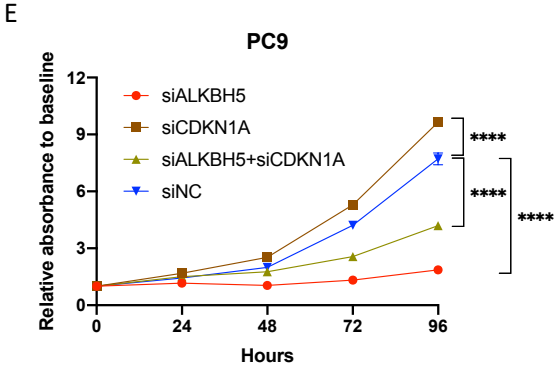
E
PC9
Relative absorbance to baseline
Hours
siALKBH5
siCDKN1A
siALKBH5+siCDKN1A
siNC
****
****
****

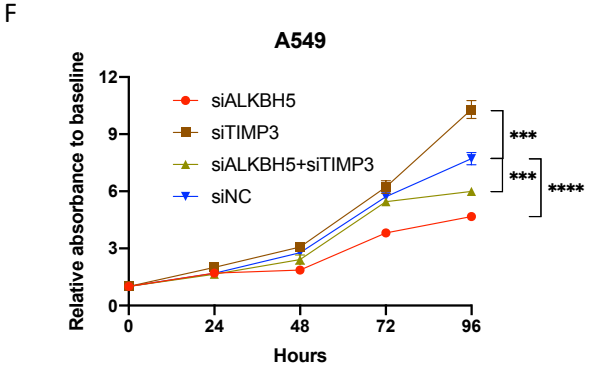
F
A549
Relative absorbance to baseline
Hours
siALKBH5
siTIMP3
siALKBH5+siTIMP3
siNC
***
***
****

Figure 8

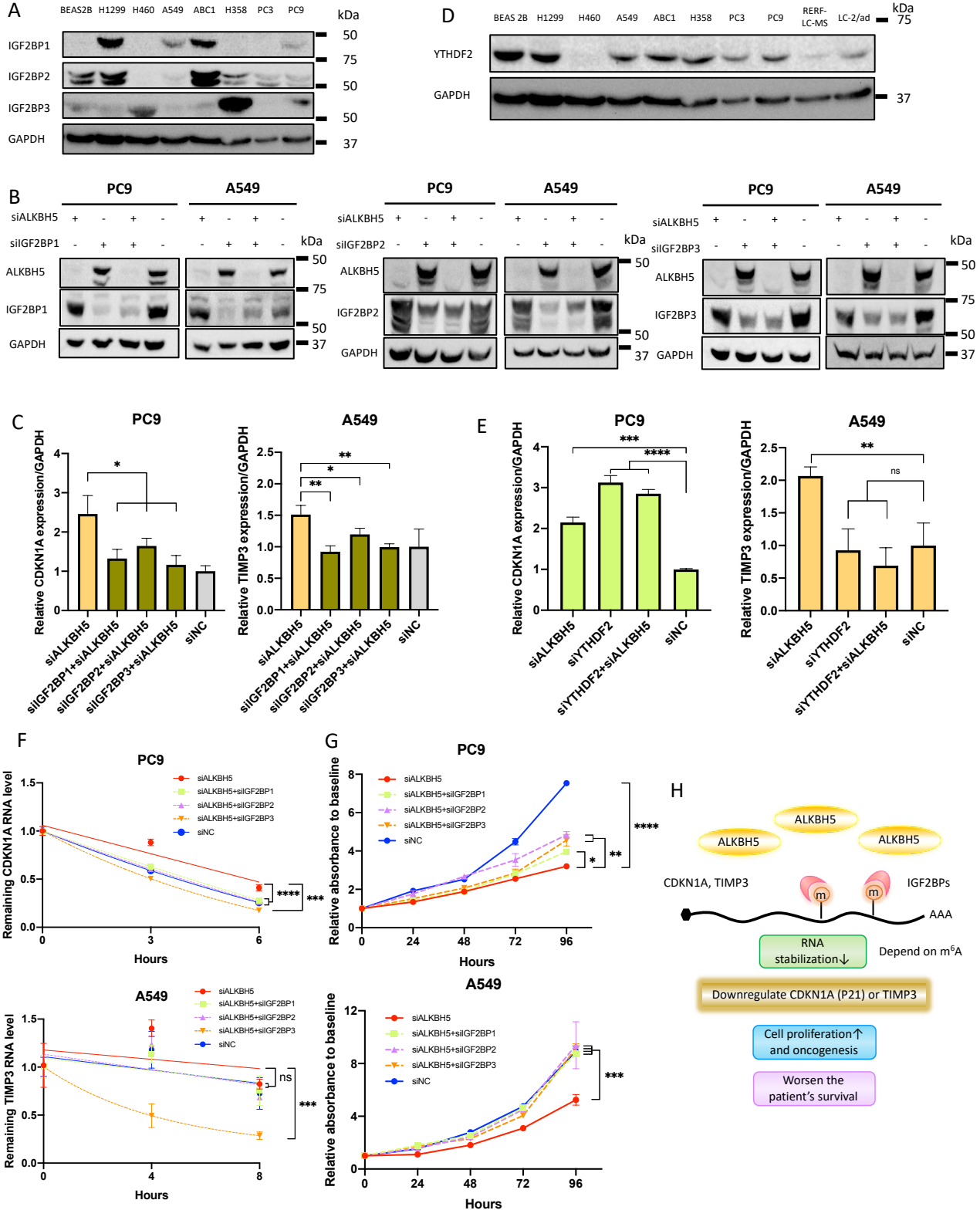
A
BEAS2B H1299 H460 A549 ABC1 H358 PC3 PC9
kDa
IGF2BP1
IGF2BP2
IGF2BP3
GAPDH
50
75
50
50
37
D
BEAS 2B H1299 H460 A549 ABC1 H358 PC3 PC9 RERF-LC-MS LC-2/ad
kDa
75
YTHDF2
GAPDH
37
B
PC9
A549
siALKBH5
siIGF2BP1
siIGF2BP2
siIGF2BP3
kDa
ALKBH5
IGF2BP1
IGF2BP2
IGF2BP3
GAPDH
50
75
50
37
C
PC9
A549
Relative CDKN1A expression/GAPDH
Relative TIMP3 expression/GAPDH
siALKBH5
siIGF2BP1+siALKBH5
siIGF2BP2+siALKBH5
siIGF2BP3+siALKBH5
siNC
E
PC9
A549
Relative CDKN1A expression/GAPDH
Relative TIMP3 expression/GAPDH
siALKBH5
siYTHDF2
siYTHDF2+siALKBH5
siNC
ns
F
PC9
A549
Remaining CDKN1A RNA level
Remaining TIMP3 RNA level
siALKBH5
siALKBH5+siIGF2BP1
siALKBH5+siIGF2BP2
siALKBH5+siIGF2BP3
siNC
Hours
G
PC9
A549
Relative absorbance to baseline
Hours
H
ALKBH5
ALKBH5
ALKBH5
CDKN1A, TIMP3
IGF2BPs
AAA
m
RNA stabilization↓
Depend on m6A
Downregulate CDKN1A (P21) or TIMP3
Cell proliferation↑ and oncogenesis
Worsen the patient's survival